

*1/11/87*

*AMES/GRANT*

THEORETICAL RESEARCH PROGRAM TO STUDY  
TRANSITION METAL TRIMERS AND EMBEDDED CLUSTERS

*ANALYTIC  
IN-25*

*(1+2)*

*CR*

*80P*

✓  
Semi-Annual Report

for  
Cooperative Agreement NCC2-296

for the period  
July 1, 1986 - December 31, 1986

Submitted to

National Aeronautics and Space Administration  
Ames Research Center  
Moffett Field, California 94305

Computational Chemistry Branch  
Dr. David Cooper, Chief and Technical Monitor

Thermosciences Division  
Dr. Jim Arnold, Chief

Prepared by

ELORET INSTITUTE  
1178 Maraschino Drive  
Sunnyvale, CA 94087  
Phone: 408 730-8422  
Telex [WU Easylink]: 62958703

K. Heinemann, President and Grant Administrator  
Stephen P. Walch, Principal Investigator

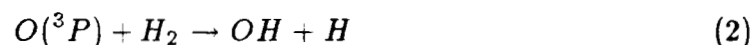
{NASA-CR-180138} THEORETICAL RESEARCH  
PROGRAM TO STUDY TRANSITION METAL TRIMERS  
AND EMBEDDED CLUSTERS Serial Annual Report, 1  
Jul. - 31 Dec. 1986 (Eloret Corp.) 80 p

CSSL 07D G3/25

N87-16084  
THRU  
N87-16086  
Unclass  
43361

In this six month period some work has continued on transition metal trimers, but most of the research effort has been redirected toward the calculation of potential energy surfaces for chemical reactions. This new emphasis reflects the importance of being able to compute, from first principles, reaction rate constants for applications related to the design of the National Aerospace Plane (NASP) and Aeroassisted Orbital Transfer Vehicles (AOTV's). Two groups of reactions are being considered.

The first set of reactions is a subset of the reactions important in  $H_2$  combustion. These reactions are important in the design of the Supersonic Combustion RAM (SCRAM) jet engine for the NASP. Among reactions which are being studied here are:



The combustion of  $H_2$  in the SCRAM jet engine involves three steps. Initiation requires production of H or O atoms. Radical propagation then occurs for H atoms via reaction (1) or for O atoms via reaction (2). OH radicals produced by reactions (1) or (2) react further via reaction (3). These reactions lead to the production of radicals in the combustor region of the SCRAM jet engine. The third step, which occurs in the nozzle region of the SCRAM jet engine, is radical recombination. Among reactions which are important here are:



Since these reactions evolve a considerable amount of heat, the rates are critical to computation of the net thrust production of the engine. The rates of these recombination reactions are slow compared to the residence time in the nozzle region, and

the rates are not well known; thus, the computed rates for these reactions are crucial to the design of the SCRAM jet engine. In collaboration with P. R. Taylor, it is planned to study reaction (4) with  $M = H_2O$ .

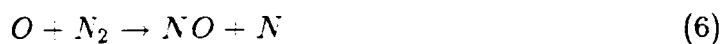
Calculations have been completed for reaction (2) and are currently underway for reaction (1). The work on reaction (2) is described in detail elsewhere[1]. The calculations on reaction (2) focused on the problem of obtaining an accurate barrier height. Previous work by Walch et al. on reaction (2) using the POL-CI method had given a barrier height of 12.5 kcal/mole, but attempts to improve upon this result by simple multi-reference singles and doubles CI methods lead to a barrier height of 16.0 kcal/mole. From comparison of computed and experimental thermal rates using the POL-CI surface, it was concluded that the 12.5 kcal/mole POL-CI barrier height is accurate. Similar results are seen for  $F + H_2$  where first order CI gave a barrier height of 1.66 kcal/mole, but multi-reference singles and doubles CI leads to barrier heights greater than 3.2 kcal/mole.

The problem of computing the barrier height for these reactions is found to be related to the problem of computing the electron affinity of the O and F atoms. Ionic character is important in the saddle point and products regions but not in the reactants regions for these reactions. In these calculations, the convergence of the barrier height was studied as a function of expanding the active space in the CASSCF calculation as well as expanding the basis set. It was found that inclusion of  $2p \rightarrow 2p'$  terms, which improve the description of the electron affinity of the O and F atoms, lowers the barrier height for the  $O + H_2$  and  $F + H_2$  reactions. It was also found that the good barrier height obtained using POL-CI results from a cancellation of opposing effects; the neglect of angular correlation in the POL-CI favors the saddle point region over reactants while the neglect of ionic terms in the POL-CI favors the reactants over the saddle point region. The calculation on

$O + H_2$  serves as an important benchmark for reactions involving O atoms. In collaboration with C. W. Bauschlicher, Jr., P. R. Taylor, and S. L. Langhoff similar calculations are currently being carried out for the  $F + H_2$  reaction.

For reaction (1) multi-reference singles and doubles CI calculations have been carried out along the minimum energy path for the addition of H atom to  $O_2$  determined in the POL-CI studies of Dunning et al. The barrier to H atom addition is found to be less than 0.3 kcal/mole, in agreement with the earlier POL-CI work. Calculations are also being carried out for the process of dissociating  $HO_2$  to  $OH + O$ . In collaboration with C. F. Melius and C. Rohlffing of Sandia laboratories it is planned to generate a global potential surface for this reaction.

The second set of reactions which are being studied are the reactions:



These reactions are important in high temperature air chemistry. Two areas where these reactions are expected to be important are i) the computation of the composition of the gas at the inlet to the SCRAM jet for the NASP and ii) the chemistry occurring in the shock layer in front of the AOTV. The details of this work are described elsewhere[2]. Calculations for these reactions are essentially complete. M. Pattengill and R. L. Jaffe are currently working on fitting the computed points. As soon as a fit has been obtained the surface will be tested by computing thermal rate constants. The surface will then be used to compute rates under non-equilibrium conditions such as occur in AOTV applications.

In the area of transition metals, work has continued on the  $Ni_3$  molecule[3]. An important problem in this area has been the difficulty in doing spectroscopy on these molecules. These difficulties arise because the small binding energies of

these molecules lead to predissociation in most of the excited states. In a previous semiannual report it was mentioned that calculations on  $\text{Cu}_3$  found a 3s Rydberg upper state which has a large transition moment connecting it with the ground state. This state was assigned as the upper state in the spectrum observed by Morse and Smalley. For  $\text{Cu}_3$  this assignment was complicated by the presence of other states arising from the  $4s^2 3d^9$  state of the Cu atom, but the 3s Rydberg upper state assignment has been supported by Morse, based on an analysis of his spectrum along with new spectral results from the dispersion fluorescence spectrum of Rohlfing and Valentini. For  $\text{Ni}_3$  the corresponding transition is computed to be at 3.0 eV in good agreement with the work of Gole who finds a strong transition in  $\text{Ni}_3$  at 2.8 eV. In addition, Gole has measured the symmetric stretch and bending frequencies of the ground state of  $\text{Ni}_3$  and these frequencies are found to be in good agreement with the calculated values for the lowest computed state of  $\text{Ni}_3$ . As an extension of this work calculations have been started to study the excited states of the  $\text{Ag}_3$  molecule, since there are unpublished spectroscopic studies on this molecule.

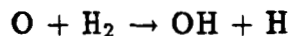
In addition to the work described here, several collaborative projects have been undertaken with other members of the Ames computational chemistry group. One such project was the calculation of the potential curves for the low-lying  $^3\Pi_u$  and  $^3\Sigma_g^-$  states of  $\text{Al}_2$ [4]. Another related project involved computing the electronic structure of the lowest few states of linear and T shaped  $\text{CuAl}_2$ [5].

### current publications

1. Extended Active Space CASSCF/MRSD CI Calculations of the Barrier Height for the Reaction:  $O + H_2 \rightarrow OH + H$ , S. P. Walch, J. Chem. Phys., submitted.
2. Calculated Potential Surfaces for the Reactions:  $O + N_2 \rightarrow NO + N$  and  $N + O_2 \rightarrow NO + O$ , S. P. Walch and R. L. Jaffe, J. Chem. Phys., submitted
3. Computed Potential Surfaces for Six Low-Lying States of  $Ni_3$ , S.P. Walch, J. Chem. Phys., submitted
4. Accurate Ab Initio Calculations Which Demonstrate a  $^3\Pi_u$  Ground State for  $Al_2$ , C.W. Bauschlicher, Jr., H. Partridge, S. R. Langhoff, P. R. Taylor, and S. P. Walch, J. Chem. Phys., submitted
5. Mixed Cu-Simple Metal Dimers and Trimers:  $CuLi$ ,  $CuLi_2$ ,  $CuNa$ ,  $CuK$ ,  $CuBe$ ,  $CuBe_2$ ,  $Cu_2Be$ ,  $CuAl$ , and  $CuAl_2$ , C. W. Bauschlicher, Jr., S. R. Langhoff, H. Partridge, and S. P. Walch, J. Chem. Phys., submitted

Items 1. and 2. are attached as  
Appendix 1 and 2, respectively.

**Extended Active Space CASSCF/MRSD CI Calculations  
of the Barrier Height for the Reaction:**



Stephen P. Walch<sup>a</sup>

Eloret Institute  
Sunnyvale, CA 94087

**Abstract**

The convergence of the barrier height for the  $\text{O} + \text{H}_2 \rightarrow \text{OH} + \text{H}$  reaction has been studied as a function of the size of the active space and basis set completeness. The barrier height is rapidly convergent with respect to expansion of the active space. Addition of  $2p \rightarrow 2p'$  correlation terms to the active space lowers the barrier to the  $\text{O} + \text{H}_2$  reaction by about 2.0 kcal/mole, but addition of 3d and other terms has little additional effect. Multireference singles and doubles contracted CI plus Davidson's correction calculations using a  $[5s5p3d2f1g/4s3p2d1f]$  basis set with a  $5\sigma 2\pi$  active space lead to a barrier height of 12.7 kcal/mole. Including an estimate of the CI contraction error and basis set superposition error leads to 12.4 kcal/mole as the best estimate of the barrier height.

<sup>a</sup>Mailing Address: NASA Ames Research Center, Moffett Field, CA 94035.

## I. Introduction

The national aerospace plane(NASP) will be an air breathing hypersonic flight vehicle capable of achieving velocities as high as Mach 25.0. It will utilize supersonic combustion ramjet( scramjet) engines and burn hydrogen for fuel. The high flow velocities introduce design difficulties, since the flame propagation speed may not be as large as the flow velocity i.e. the flame may blow out. This has resulted in considerable interest in the kinetics of reactions involving H, O, and N. Recently a research program has been started to compute from first principles the rates of selected reactions important in SCRAM jets. The computation of the rate of these reactions first entails the computation of the potential energy surfaces for the reactions of interest.

In order to assess the accuracy of potential energy surfaces involving oxygen, a systematic study was carried out of the convergence of the barrier height for the  $O + H_2 \rightarrow OH + H$  reaction as a function of both the size of the active space in the CASSCF calculation and the size of the basis set. This reaction was selected for study since a number of dynamics studies[1-4] have been carried out based on the POL-CI surface of Walch et al.[5]. The agreement between the computed and the experimental thermal rate constants establish that the barrier height of 12.5 kcal/mole from the POL-CI surface is accurate to better than 1.0 kcal/mole. We also note here that a similar study by Howard et al.[6] using a first order CI iterative natural orbital procedure led to a barrier height of 14.0 kcal/mole.

Although the POL-CI barrier height is believed to be quite accurate, the computed endoergicity( $\Delta E_{rx}$ ) on the other hand is -0.1 kcal/mole compared to an experimental value of +2.9 kcal/mole. Thus, one has to assume that the good result for the computed barrier height is somewhat fortuitous. As discussed in Section III., attempts to improve upon the POL-CI result by using multireference singles



and doubles CI methods (MRSD CI) lead to a barrier of 16.0 kcal/mole using the same three reference configurations and a comparable basis set to that used in the POL-CI study. Similarly, for the  $F + H_2$  reaction a first order CI calculation by Bender and coworkers[7] gave a barrier height of 1.66 kcal/mole, but more recent calculations using MRSD CI and perturbation theory methods have lead to barriers greater than 3.2 kcal/mole even when very large basis sets are used[8].

In the present paper we examine the source of the differences between the POL-CI and MRSD-CI calculations. For both of these reactions, ionic terms are expected to be important in the saddle point and products regions but not in the reactants region. Thus, the problem of describing the barrier height for these reactions is closely related to the problem of describing the electron affinity of the O and F atoms. Botch and Dunning[9] found that  $2p \rightarrow 2p'$  terms were important in describing the O and F atom electron affinities. For example, with the largest basis set used in the present studies, the computed electron affinity for O is 1.27 eV for a MRSD-CI calculation based on a CASSCF including  $2p \rightarrow 2p'$  correlation. This number may be compared to 1.46 eV for experiment[10] and 1.04 eV for SCF plus singles and doubles CI with a very large basis set[11]. Thus, it is seen that  $2p \rightarrow 2p'$  correlation is very important in describing the electron affinity of O atom, and these terms were added to the active space in these calculations.

Section II describes the basis sets and the computational approach. Section III presents the results of calculations using an expanded active space and extended basis sets, while the conclusions are presented in Section IV.

## II. Computational Details.

Table I gives the O basis sets which were used in this study. The O sp basis set is a [5s3p] segmented contraction of the van Duijneveldt (11s6p) primitive set[12]. The inner nine primitive functions were contracted (63) based on the 1s orbital, while

the outer five s functions were contracted (311) based on the 2s orbital. (Note that this contraction uses three functions twice.) In order to describe  $O^-$  character, the basis set was augmented by a single set of 2p functions with the exponent selected using an even tempered criterion leading to a [5s4p] sp basis set. The polarization function basis sets were developed from the gaussian fits to Slater type orbitals given by Stewart[13]. In each case the effective Slater exponent was optimized at the CI level using a two term GTO fit[13] to a Slater. The exponent for the O3d function was optimized at the CI level for the ground state of the O atom, while the exponents for the O4f and O5g were optimized at the CI level for the OH molecule.

The H basis set is given in Table II. The hydrogen s basis set used the van Duijneveldt 6s set[12] contracted to [3s] plus one diffuse function selected in an even tempered fashion. The [2p] basis set was selected as a four term fit[13] to a 2p STO with exponent of 1.0. This primitive basis was contracted (211) and the most diffuse function was discarded leading to a [4s2p] basis set, which was used for the smallest basis set for  $O + H_2$ . The scale factor of the H p function was subsequently optimized at the SDCI level for  $H_2$  using a [4s1p] basis set. This lead to an effective 2p Slater exponent of 1.84. The [4p] basis was generated from this Slater exponent as a 211 contraction of a 4 term STO[13] plus one diffuse 2p function selected by an even tempered criterion. A [3p] set was also used which consisted of the [4p] set minus the most diffuse exponent. The 3d and 4f exponents used here were optimized at the CI level for OH. From these s, p, d, and f basis functions five different basis sets were generated: [4s2p], [4s3p1d], [4s4p1d], [4s4p2d], and [4s4p2d1f].

During the course of this work, Almlöf and Taylor implemented a new version of the molecule integral program which permits general contractions. These authors also developed basis sets for use with this program in which the occupied and virtual orbitals are generally contracted based on the natural orbitals

from an atomic CI calculation[14]. These basis sets are optimal for describing the atomic correlation and thus have very small basis set superposition errors. In addition the basis sets are found to be sufficiently flexible to be used in molecular calculations at both the SCF and CI level. In the present studies a (13s9p6d4f2g/8s6p4d3f)/[5s5p3d2f1g/4s3p2d1f] basis set[14] was used. Here the fifth O2p function was a diffuse function to describe O<sup>-</sup> character. This last function was selected using an even tempered criterion. This basis set is referred to as the atomic natural orbital (ANO) basis set.

Most of the calculations were carried out on the CRAY XMP-48 with the MOLECULE[15]-SWEDEN[16] system of programs. Some of the basis set tests were carried out on the Cyber-205 using the Karlsruhe adaptation[17] of the COLUMBUS[18] codes. These calculations used the Coupled Pair Functional(CPF) method of Ahlrichs[19].

Since the CI calculations reported here use a limited set of reference configurations, the CI energy is not invariant to a unitary transformation of the CASSCF orbitals among themselves. The CASSCF active orbitals are uniquely defined by a natural orbital transformation of the converged active orbitals, followed by a CASSCF CI in the natural orbital basis to define the important reference configurations.

Most of the CI calculations presented here were uncontracted; however, some calculations were carried out with the externally contracted CI of Siegbahn[20]. Calculations which use the contracted CI are denoted by CCI while the uncontracted calculations are denoted by CI. In all cases the multireference analog of Davidson's correction[21] was computed and results are reported both with and without Davidson's correction. The correction used in the CCI is  $\Delta E (1 - C_0^2)/C_0^2$  which differs slightly from the original Davidson's correction, used in the uncontracted CI, which

is  $\Delta E (1 - C_0^2)$ , where  $\Delta E$  is the CI energy minus the reference energy and  $C_0^2$  is the square of the coefficient of the reference configuration or the sum of the squares of the coefficients of the reference configurations in the multireference case. The results where Davidson's correction has been applied are denoted by CI + Q or CCI + Q for the uncontracted and contracted CI, respectively. All of the calculations were performed for collinear geometries using  $C_{2v}$  symmetry.

### III. Discussion.

For collinear geometries, the SCF configuration of the reactants  $O + H_2$  on the  $^3\Pi$  surface is:

$$1\sigma^2 2\sigma^2 3\sigma^2 4\sigma^1 1\pi_x^2 1\pi_y^1 \quad (1)$$

Here  $1\sigma$  and  $2\sigma$  are  $O1s$  and  $O2s$  like orbitals. The  $3\sigma$  orbital is the  $H_2$  bonding orbital ( $1\sigma_g$ ) and the  $4\sigma$  and  $1\pi$  orbitals are the  $O2p$  orbitals. As described elsewhere[5], the  $3\sigma$  and  $4\sigma$  orbitals map into the  $OH\sigma$  bonding orbital and a  $H1s$  orbital for the products. In order to describe the spin recoupling process it is necessary to also include the configurations.

$$1\sigma^2 2\sigma^2 3\sigma^1 4\sigma^1 5\sigma^1 1\pi_x^2 1\pi_y^1 \quad (2)$$

$$1\sigma^2 2\sigma^2 4\sigma^1 5\sigma^2 1\pi_x^2 1\pi_y^1 \quad (3)$$

where the  $5\sigma$  orbital corresponds to the  $H_2 1\sigma_u$  orbital. The three configurations above were the reference configurations in the POL-CI calculations of Walch et al.[5].

Table III shows the calculated barrier height and endoergicity obtained using CASSCF orbitals for a  $3\sigma 1\pi$  active space and a CCI with eqn. 1-3 as reference configurations ([5s4p2d1f/4s2p] basis set). Looking first at the results correlating eight electrons, it is seen that the computed barrier height and endoergicity are both

too large. Since the saddle point and products regions both contain an  $O^-$  term that is not present for reactants, this problem is probably related to the difficulty in calculating the electron affinity of O atom at the SCF level. For both saddle point and products regions, quadruple excitations, which arise as products of correlation terms needed to describe the transfer of the  $H_2$  bond pair and correlation terms for describing  $O^-$  character, are important. These terms may be somewhat less important for the products region, since the bond pair has relocated. As will be seen later, this hypothesis is supported by the lowering of the barrier height when these higher excitations are explicitly included by expanding the reference space in the expanded active space CI calculations.

From Table III it is also seen that, at this level of calculation, a better endoergicity is obtained if the  $O2s$  electrons are not correlated. This is in accord with calculated  $D_e$ 's for the  $O_2$  molecule where better results are obtained, when the  $O2s$  electrons are inactive in the CASSCF calculation, if the  $O2s$  levels are not correlated in the CI calculation[22]. As will be seen later, with larger basis sets and a more complete correlation treatment, the eight electron endoergicity is in better agreement with the experimental value. For the  $[5s4p2d1f/4s2p]$  basis set, the calculated barrier height is the same at the CI + Q level whether six electrons or eight electrons are correlated. Thus, the calculations to determine the size of the active space, which used this basis set, were carried out with only six electrons correlated.

Since  $O^-$ -like terms are expected to be important in the saddle point region, the CASSCF active space was expanded to include the most important of these terms. In the present studies the active space was expanded by addition of the  $O2p'$  natural orbitals, where the  $2p'$  is a tight-diffuse correlating orbital (i.e. it has an extra radial node like a  $3p$  orbital but is of the same radial extent as a  $2p$  orbital), the  $O3d$  natural orbitals, and the  $H_2$   $2\sigma_g$  and  $1\pi_u$  natural orbitals, where

the orbital notation refers to the reactant geometry. For the  $\sigma$  orbitals, the order of these natural orbitals (in order of decreasing natural orbital occupation numbers) is the same for both the reactants and saddle point geometries:

$$H_2 1\sigma_g > O_2 p\sigma > H_2 1\sigma_u > H_2 2\sigma_g > O_2 p\sigma' > O_3 d$$

For the  $\pi$  orbitals on the other hand the order is different for reactants and saddle point geometries. The order for reactants is:

$$O_2 p\pi > O_2 p\pi' > H_2 1\pi_u > O_3 d$$

while for the saddle point region the order is:

$$O_2 p\pi > O_2 p\pi' > O_3 d > H_2 1\pi_u$$

From the above one sees that in order to include the  $O_2 p'$  shell consistently it is necessary to use a  $5\sigma 2\pi$  active space. To consistently add the  $O_3 d$  shell would require a  $6\sigma 4\pi 1\delta$  active space.

The effect of adding additional active orbitals was tested at the CCI level by systematically expanding the CASSCF active space while adding corresponding reference configurations. The smallest active space is  $3\sigma 1\pi$  which corresponds to the configurations given in eqn. 1-3. The  $4\sigma 2\pi$  active space adds the  $O_2 p\sigma'$  and  $O_2 p\pi'$  orbitals. The  $5\sigma 3\pi$  active space adds the  $H_2 2\sigma_g$  like and  $O_3 d\pi$  like natural orbitals. Finally, the  $6\sigma 3\pi$  active space had the same  $\pi$  space as the  $5\sigma 3\pi$  case, but the  $3d\sigma$  like natural orbital was added to the  $\sigma$  active space.

The reference configurations for the MRSD CCI calculations included 1-3 and added 4-7.

$$1\sigma^2 2\sigma^2 3\sigma^2 4\sigma^1 2\pi_x^2 1\pi_y^1 \quad (4)$$

$$1\sigma^2 2\sigma^2 3\sigma^1 5\sigma^1 n\sigma^1 1\pi_x^2 1\pi_y^1 \quad (5)$$

$$1\sigma^2 2\sigma^2 3\sigma^1 4\sigma^1 5\sigma^1 1\pi_x^1 l\pi_x^1 1\pi_y^1 \quad (6)$$

$$1\sigma^2 2\sigma^2 3\sigma^1 4\sigma^1 5\sigma^1 1\pi_x^2 m\pi_y^1 \quad (7)$$

In 5-7  $n$  runs from 6 to the total number of  $\sigma$  orbitals and  $l$  and  $m$  run from 2 to the total number of  $\pi$  orbitals. Eqn. 4 corresponds to the diagonal double  $2p \rightarrow 2p'$  excitation, while 5-7 are interpair terms between the  $H_2$  bond pair and the  $2p \rightarrow 2p'$  excitations. This choice of reference configurations includes all configurations with CI coefficients greater than 0.05 in the CASSCF wavefunction. The barrier height was computed in each case with and without Davidson's correction[21] with the reactants limit referenced to the  $6\sigma 3\pi$  reactants energy. The energy reference was chosen in this way since the reactants energy was relatively insensitive to expansion of the active space (the effect of expanding the active space is only 0.3 kcal/mole at the reactants geometry) and the resulting values of the barrier height,  $\Delta E_b$ , then reflect the convergence of the total energy at the saddle point geometry.

Table IV shows the effect of expanding the active space in the CASSCF calculation. Adding the  $2p'$  shell has a large differential effect on the barrier height, but addition of further active orbitals has only a relatively small effect. This is consistent with the idea that configurations involving the  $2p'$  shell are the most important correlation terms needed to describe  $O^-$ . Based on these calculations a  $5\sigma 2\pi$  active space was used in subsequent calculations to determine the saddle point properties for  $O + H_2$ . The reference configurations that were used in these calculations are given in Table V. The configurations in Table V include a diagonal double  $3\sigma^2 \rightarrow 6\sigma^2$  which is the  $H_2$   $1\sigma_g^2 \rightarrow 2\sigma_u^2$  and which was not included in the set of configurations given above. In addition, the configuration given in eqn(5) for  $n=6$  is found to be unimportant and is omitted.

A grid of points was computed about the expected saddle point and the actual saddle point geometry was determined by fitting these data to a function of the form:

$$F(r_1, r_2) = c_0 + c_1 r_1 + c_2 r_2 + c_3 r_1 r_2 + c_4 r_1^2 + c_5 r_2^2 \quad (8)$$

Here the saddle point was determined both for CI and CI + Q. At the reactants geometry, the H<sub>2</sub> distance was optimized for an O + H<sub>2</sub> supermolecule calculation.

Table VI shows the results of MRSD CI calculations for O + H<sub>2</sub> using the [5s4p2d1f/4s2p] basis set and a 5 $\sigma$ 2 $\pi$  active space as described above. The saddle point geometry obtained here has  $r_{OH}$  0.01  $a_0$  shorter and  $r_{HH}$  0.06  $a_0$  shorter than the values determined for the POL-CI calculations. The present studies also show a larger curvature in the direction along the reaction coordinate. Based on a Wigner correction[23] for tunneling, the larger curvature would indicate tunneling is more important on the CI surface than on the POL-CI surface. The barrier height obtained for the 5 $\sigma$ 2 $\pi$  active space is 2.1 kcal/mole lower than obtained with the 3 $\sigma$ 1 $\pi$  active space( see table III). This is a very significant effect strongly suggesting that O<sup>-</sup>-like terms are very important for the O + H<sub>2</sub> reaction.

An additional calculation was carried out at the saddle point geometry from Table VI using the 5 $\sigma$ 2 $\pi$  active space CASSCF but with additional reference configurations. The new reference configurations included: i) selected triple and quadruple excitations which arise as products of the diagonal double excitation 3 $\sigma^2 \rightarrow 5\sigma^2$  and 2p  $\rightarrow$  2p' single and double excitations and ii) atomic interpair terms which are double 2p  $\rightarrow$  2p' excitations. Inclusion of these addition reference configurations increases the barrier height very slightly (0.1 kcal/mole). This result indicates that the calculation is essentially converged with respect to the list of reference configurations.

Table VII shows two important effects on the barrier height for the O + H<sub>2</sub> reaction as a result of expanding the basis set. The first is that correlating the O2s lowers the barrier by only 0.1 kcal/mole with the [5s4p2d1f/4s2p] basis set, but by 0.5 kcal/mole for the [5s4p3d2f1g/4s3p1d] basis set. The second effect illustrated in Table VII is the importance of higher angular momentum functions for these CPF



wave functions. For the case of correlating eight electrons one sees a 1.1 kcal/mole lowering of the barrier height for the [5s4p3d2f1g/4s4p2d1f] basis set compared to the [5s4p2d1f/4s2p] basis set. For the largest basis set the CPF barrier height is 13.6 kcal/mole when eight electrons are correlated (Table VII). Correcting for the basis set superposition error leads to a CPF barrier height of 14.3 kcal/mole.

Table VIII shows the results of CCI calculations with the ANO basis set. Here it is seen that the barrier height is 14.7 kcal/mole for CCI and 12.7 kcal/mole for CCI + Q when eight electrons are correlated. For these calculations it was necessary to use the contracted CI, since the calculation involves about 1.2 million configurations (uncontracted). For the calculation with the [5s4p2d1f/4s2p] basis set and  $5\sigma 2\pi$  active space the contraction error is found to be 0.5 kcal/mole when six electrons are correlated. The superposition error for the ANO basis set is calculated by the counterpoise method to be 0.15 kcal/mole when eight electrons are correlated. Combining these numbers leads to an estimate of 14.4 kcal/mole and 12.4 kcal/mole for CI and CI + Q, respectively. Since the multireference Davidson's correction may be an overestimate, we can only say with confidence that the computed barrier height is within 2.0 kcal/mole of the currently accepted value of 12.5 kcal/mole; although, the true error is probably about half that large. Table VIII also shows the computed endoergicity. Here it is seen that the error is 0.9 kcal/mole for CCI and 1.6 kcal/mole for CCI + Q. These errors are seen to be of the same order of magnitude as the estimated error in the barrier height.

Table VIII also shows the computed barrier height with respect to the OH + H products. The result for CCI + Q correlating eight electrons is 8.2 kcal/mole as compared to the experimentally derived value of 9.6 kcal/mole (the 12.5 kcal/mole barrier height minus the experimental endoergicity). This result indicates that the multireference Davidson's correction must be overshooting to some extent, since the

CCI + Q barrier height is 0.1 kcal/mole and 1.4 kcal/mole lower than "experiment" for the forward and reverse directions, respectively. It should be noted that the barrier height for the reverse reaction is not corrected for superposition error or the CCI contraction error.

A remarkable result of these studies is that the present calculations which involve more than 1.2 million configurations are finally converging toward the barrier height obtained in the POL-CI calculations which involved only a few thousand configurations. It is clear from the present studies that the POL-CI calculations, which allow only one electron outside the  $3\sigma 1\pi$  active space, cannot properly describe the  $O^-$  character in the wavefunction at the saddle point geometry, since these studies show that a larger active space ( $5\sigma 2\pi$ ) is needed for that purpose. Thus, one might have expected that the POL-CI method would result in too large a barrier height as was obtained in the CCI studies using a  $3\sigma 1\pi$  active space. The POL-CI treatment neglects the angular and radial correlation of the  $H_2$  molecule which is expected be more important for reactants than for the saddle point region. However, the neglected ionic terms are less important for the reactants than for the saddle point region. Thus, it appears that an accidental cancellation of these opposing effects accounts for the good barrier height obtained in the POL-CI. Adding additional correlation to this wavefunction by allowing single and double excitations from the POL-CI reference set leads to a higher barrier, since angular and radial correlation is easy to describe, but a larger active space and extended basis set treatment is necessary to properly describe  $O^-$  character. It is only after inclusion of extended basis sets and active spaces that a balanced description and lower barrier height are obtained, as in the present calculation.

#### IV. Conclusions.

The convergence of the barrier height for the  $O + H_2 \rightarrow OH + H$  reaction has

been studied as a function of the size of the active space and basis set completeness. The barrier height is found to be rapidly convergent with respect to expansion of the active space. Addition of  $2p \rightarrow 2p'$  correlation terms to the active space lowers the barrier to the  $O + H_2$  reaction by about 2.0 kcal/mole, but addition of 3d and other terms has little additional effect. Since the saddle point region of this reaction is expected to have a significant  $O^-$  component which will not be important for the reactants, these results suggest that the difficulty in accurately computing the barrier height for the  $O + H_2$  reaction parallels the problem of describing the electron affinity of oxygen. Multireference singles and doubles contracted CI plus Davidson's correction calculations using a  $[5s5p3d2f1g/4s3p2d1f]$  basis set with a  $5\sigma 2\pi$  active space lead to a barrier height of 12.7 kcal/mole. Including an estimate of the CI contraction error and basis set superposition error leads to 12.4 kcal/mole as the best estimate of the barrier height. The latter result is in good agreement with the current estimate of 12.5 kcal/mole.

#### ACKNOWLEDGMENTS

S.P. Walch was supported by a NASA grant(NCC2-296). The author is indebted to Dr. Peter Taylor for providing the ANO basis set used in these studies. Helpful discussions with Dr. Richard Jaffe and Dr. Peter Taylor are gratefully acknowledged.

## References

1. S.P. Walch, A.F. Wagner, T.H. Dunning, Jr., and G.C. Schatz, J. Chem. Phys., **72**, 2894(1980).
2. G.C. Schatz, A.F. Wagner, S.P. Walch, and J.M. Bowman, J. Chem. Phys., **74**, 4984(1981).
3. K.T. Lee, J.M. Bowman, A.F. Wagner, and G.C. Schatz, J. Chem. Phys., **76**, 3583(1982).
4. B.C. Garrett, D.G. Truhlar, and G.C. Schatz, J. Amer. Chem. Soc., **108**, 2876(1986).
5. S.P. Walch, T.H. Dunning, Jr., R.C. Raffanetti, and F.W. Bobrowicz, J. Chem. Phys., **72**, 406(1980).
6. R.E. Howard, A.D. McLean, and W.A. Lester, Jr., J. Chem. Phys., **71**, 2412(1979).
7. C.F. Bender, S.V. O'Neil, P.K. Pearson, and H.F. Schaefer III., Science, **176**, 1412(1972).
8. M. J. Frisch, B. Liu, J.S. Binkley, H.F. Schaefer III., and W.H. Miller, Chem. Phys. Lett., **114**, 1(1985).
9. B.H. Botch and T.H. Dunning, Jr., J. Chem. Phys., **76**, 6046(1982).
10. H. Hotop and W.C. Lineberger, J. Phys. Chem. Ref. Data, **4**, 539(1975).
11. F. Sasaki and M. Yoshimine, Phys. Rev. A9, **17**, 26(1974).
12. F.B. van Duijneveldt, IBM Technical Research Report No. RJ945(1971).
13. R.F. Stewart, J. Chem. Phys., **52**, 431(1970).
14. J. Almlöf and P.R. Taylor, J. Chem. Phys., submitted.
15. J. Almlöf, MOLECULE, a Gaussian integral program.

16. P.E.M. Siegbahn, C.W. Bauschlicher, Jr., B. Roos, A. Heiberg, P.R. Taylor, and J. Almlöf, SWEDEN, A vectorized SCF MCSCF direct CI.
17. The codes have been modified and vectorized for the Cyber 205 by R. Ahlrichs and coworkers.
18. The Columbus codes include the Gaussian integral program of R. Pitzer and the unitary group CI codes of I. Schavitt, F. Brown, H. Lischka, and R. Shepard.
19. R. Ahlrichs, S. Scharf, and C. Ehrhardt, J. Chem. Phys., **82**, 890(1985).
20. P.E.M. Siegbahn, Int. J. Quantum Chem., **23**, 1869(1983).
21. S.R. Langhoff and E.R. Davidson, Int. J. Quantum Chem., **8**, 61(1974).
22. S.P. Walch and R.L. Jaffe, J. Chem. Phys., submitted
23. E.P. Wigner, Z. Phys. Chem. Abt., **B19**, 203(1932).

Table I. Basis Sets for Oxygen.

O [5s4p] valence basis		
function	s	p
1	31195.560(0.00021)	64.7719(0.00584)
2	4669.3800(0.00163)	14.9727(0.04058)
3	1062.2600(0.00845)	4.55440(0.15754)
4	301.42600(0.03419)	1.56370(0.35300)
5	98.515300(0.11031)	0.54107(1.00000)
6	35.460900(0.26949)	0.17776(1.00000)
7	13.617900(0.42355)	0.05840(1.00000)
8	5.3862000(0.28304)	
9	1.5387000(0.02748)	
7	13.617900(-.14601)	
8	5.3862000(-.14788)	
9	1.5387000(0.23867)	
10	0.605500(1.00000)	
11	0.220500(1.00000)	

[3d2f1g] polarization basis			
function	d	f	g
1	7.5130(0.05799)	5.4860(0.173786)	2.5880(0.484830)
2	2.3890(0.30456)	1.9670(0.597338)	0.9750(0.653938)
3	0.9713(1.00000)	0.8418(1.000000)	
4	0.4324(1.00000)		

[2d1f] polarization basis		
function	d	f
1	4.2770(0.16866)	1.806(0.47694)
2	1.3410(0.58480)	0.618(0.65874)
3	0.5220(1.00000)	

Table II. Basis Sets for Hydrogen.

---



---

[4s4p2d1f] Hydrogen basis				
function	s	p	d	f
1	82.63637(0.006172)	6.0760(0.05713)	3.535(0.168660)	1.204(0.476935)
2	12.40960(0.047210)	<u>1.5750(0.28575)</u>	<u>1.108(0.584798)</u>	0.412(0.658738)
3	2.823850(0.232530)	<u>0.5554(1.00000)</u>	0.432(1.000000)	
4	<u>0.797670(0.790500)</u>	<u>0.2211(1.00000)</u>		
5	<u>0.258100(1.000000)</u>	0.0880(1.00000)		
6	<u>0.089890(1.000000)</u>			
7	<u>0.030000(1.000000)</u>			

[2p1d] polarization basis		
function	p	d
1	1.7983(0.17705)	1.827(0.46662)
2	<u>0.4663(0.88560)</u>	0.548(0.66447)
3	<u>0.1644(1.00000)</u>	

Table III. Calculations for  $O + H_2 \rightarrow OH + H$   
 [5s4p2d1f/4s2p] basis set  
 3 $\sigma$ 1 $\pi$  active space

	CCI <sup>a,b</sup> , kcal/mole		
Geometry	6 electrons	8 electrons	expt.
products	3.6(3.3)	6.7(6.6)	2.9
saddle point <sup>c</sup>	17.0(16.0)	17.5(16.0)	12.5
reactants	0.0	0.0	0.0
D <sub>e</sub> (H <sub>2</sub> )	4.62	4.62	4.75
D <sub>e</sub> (OH)	4.48	4.33	4.62

<sup>a</sup> Values in parenthesis include Davidson's correction.

<sup>b</sup> All quantities are in kcal/mole except the D<sub>e</sub> values which are in eV.

<sup>c</sup> The saddle point geometry is  $r_{OH}=2.293$  and  $r_{HH}=1.764$  which is very close to the POL-CI saddle point geometry. The OH and H<sub>2</sub> bond lengths are  $r_{OH}=1.868$  and  $r_{HH} = 1.431$



Table IV. Calculations for  $\text{O} + \text{H}_2 \rightarrow \text{OH} + \text{H}$   
 [5s4p2d1f/4s2p] basis set  
 Effect of expanded active space

	$\Delta E_b^a$ , kcal/mole	
active space	CCI	CCI + Q
$3\sigma 1\pi$	17.3	15.9
$4\sigma 2\pi$	15.2	14.4
$5\sigma 3\pi$	15.1	14.3
$6\sigma 3\pi$	15.0	14.2

<sup>a</sup> Using the reactants and saddle point geometry as in Table III.

Table V. Reference Configurations for O + H<sub>2</sub>.

---



---

$1\sigma^2 2\sigma^2 3\sigma^2 4\sigma^1 1\pi_x^2 1\pi_y^1$
$1\sigma^2 2\sigma^2 3\sigma^1 4\sigma^1 5\sigma^1 1\pi_x^2 1\pi_y^1$
$1\sigma^2 2\sigma^2 4\sigma^1 5\sigma^2 1\pi_x^2 1\pi_y^1$
$1\sigma^2 2\sigma^2 4\sigma^1 6\sigma^2 1\pi_x^2 1\pi_y^1$
$1\sigma^2 2\sigma^2 3\sigma^2 4\sigma^1 2\pi_x^2 1\pi_y^1$
$1\sigma^2 2\sigma^2 3\sigma^1 5\sigma^1 7\sigma^1 1\pi_x^2 1\pi_y^1$
$1\sigma^2 2\sigma^2 3\sigma^1 4\sigma^1 5\sigma^1 1\pi_x^1 2\pi_x^1 1\pi_y^1$
$1\sigma^2 2\sigma^2 3\sigma^1 4\sigma^1 5\sigma^1 1\pi_x^2 2\pi_y^1$

Table VI. Computed Saddle Point Properties for O + H<sub>2</sub>. <sup>a</sup>

property	POL-CI	CI	CI + Q
$\Delta E_b$ , kcal/mole	12.5	14.9	13.9
$r_{OH}$ , a <sub>0</sub>	2.320	2.313	2.314
$r_{HH}$ , a <sub>0</sub>	1.747	1.690	1.688
curvature <sup>b</sup>	-0.057	-0.083	-0.078

<sup>a</sup> Multireference SDCI calculations with a  $5\sigma 2\pi$  active space and a [5s4p2d1f/4s2p] basis set.

<sup>b</sup> Negative eigenvalue of the Hessian matrix.

Table VII. Calculations for  $\text{O} + \text{H}_2 \rightarrow \text{OH} + \text{H}$

Effect of Basis Set

Basis set	$\Delta E_b^a$ , kcal/mole	
	6 electrons	8 electrons
[5s4p2d1f/4s2p]	14.83	14.72
[5s4p3d2f1g/4s3p1d]	14.73	14.20
[5s4p3d2f1g/4s4p1d]		14.09
[5s4p3d2f1g/4s4p2d]		13.87
[5s4p3d2f1g/4s4p2d1f]		13.60(14.3 <sup>b</sup> )

<sup>a</sup> CPF calculations using the saddle point and reactants geometries from the multireference SDCl calculations using a  $5\sigma 2\pi$  active space and the [5s4p2d1f/4s2p] basis set.

<sup>b</sup> Including an estimate of basis set superposition error.

Table VIII. Computed Barrier Height and Endoergicity for  $O + H_2$ .<sup>a</sup>

property	CCI(6 electrons)	CCI(8 electrons)	expt.
$\Delta E_b$ <sup>b</sup> , kcal/mole	15.1(14.0)	14.7(12.7)	
contraction error	0.5	0.5	
superposition error	(0.0)	0.15	
$\Delta E_b$ (corr.)	14.8(13.7)	14.4(12.4)	(12.5)
$\Delta E_{rx}$ , kcal/mole	1.7(1.9)	3.8(4.5)	2.9

<sup>a</sup> Multireference CCI calculations with a  $5\sigma 2\pi$  active space and a  $[5s5p3d2f1g/4s3p2d1f]$  ANO basis set.

<sup>b</sup> The computed barrier height viewed from the  $OH + H$  direction is 13.5(12.1) and 11.0(8.2) kcal/mole for correlating six electrons and eight electrons, respectively. This may be compared to 9.6 kcal/mole for "experiment".

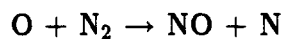
APPENDIX 2

D<sub>1</sub>-25

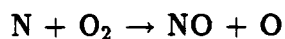
51P.

N87-16086

**Calculated Potential Surfaces for the Reactions:**



and



Stephen P. Walch<sup>a</sup>

Eloret Institute

Sunnyvale, CA 94087

and

Richard L. Jaffe

NASA Ames Research Center

Moffett Field, CA 94035

**Abstract**

Complete Active Space SCF/ Contracted CI (CASSCF/CCI) calculations, using large gaussian basis sets, are presented for selected portions of the potential surfaces for the reactions in the Zeldovich mechanism for the conversion of N<sub>2</sub> to NO. The N + O<sub>2</sub> reaction is exoergic by 32 kcal/mole and is computed to have an early barrier of 10.2 kcal/mole for the <sup>2</sup>A' surface and 18.0 kcal/mole for the <sup>4</sup>A' surface. The O + N<sub>2</sub> reaction is endoergic by 75 kcal/mole. The <sup>3</sup>A'' surface is calculated to have a late barrier of 0.5 kcal/mole, while the <sup>3</sup>A' surface is calculated to have a late barrier of 14.4 kcal/mole.

<sup>a</sup>Mailing Address: NASA Ames Research Center, Moffett Field, CA 94035.

## I. Introduction

Aeroassisted orbital transfer vehicles (AOTVs) will be designed to use the aerodynamic forces produced over the surface of a large heat shield (possibly 100 meters in diameter) to permit transfer between high and low altitude earth orbits with reduced use of rocket propulsion for maneuvering. During these orbital transfer trajectories the vehicle will be subjected to substantial radiative and convective heat transfer from the bow shock wave to the heat shield. By operating at high altitudes ( $> 70$  km), where the atmospheric density is low, convective heating is reduced, but nonequilibrium radiation enhancement[1] is significant. The air in the shock layer which forms in front of the AOTV is at sufficiently low pressure that, while the rotational and translational modes of the molecules may be equilibrated, the vibrational and electronic degrees of freedom will definitely not be equilibrated. It is reasonable to characterize the various energy modes by different temperatures. Expected values of the translational and rotational temperatures here are in the range of 10000-50000K (about 1-5 eV), while the vibrational and electronic temperatures are typically less than 15000K. The physical and chemical phenomena occurring under these conditions are poorly understood, and existing laboratory data show uncertainties of a factor of about 4 for important rate constants at the flight velocities anticipated for the AOTV[2]. Attempts are currently being made to model these processes[2-3].

Among input needed to model the characteristics of such high temperature non-equilibrium air is a kinetic data base for several classes of air reactions. Among these are i) charge transfer processes such as  $N + N^+ \rightarrow N^+ + N$  [4], dissociative processes such as  $N_2 + N \rightarrow N + N + N$  [5], and the atomic molecular exchange processes studied in the present paper:  $N + O_2 \rightarrow NO + O$ , and  $O + N_2 \rightarrow NO + N$ . Since the electronic temperature may be greater than 10000K, excited state reactions may also be important. For example at 10000K 16.4 % of the  $O_2$  molecules are in the  $^1\Delta_g$  state and 5.4 % of the O atoms and 13.3 % of the N atoms are in the  $^1D$  and  $^2D$  states, respectively. The excited electronic state reactions  $N(^2D) + O_2$  and  $N + O_2(^1\Delta_g)$  are believed to be faster than the corresponding ground state reactions at low temperatures[6]. They occur on potential energy surfaces which directly connect to ground state products with little or no activation

barriers and are also highly exothermic. At high temperatures, however, the rate constants will be limited by the overall collision rate which should be nearly the same for each reaction. In the case of the  $\text{N}_2 + \text{O}(^1\text{D})$  reaction, the adiabatic potential energy surfaces lead to electronically excited products ( $\text{NO}^2\Pi + \text{N}(^2\text{P})$ ) and contain a deep energy minimum corresponding to the stable  $\text{N}_2\text{O}$  molecular electronic ground state. It is not believed that this highly endothermic reaction will make a significant contribution to the rate constants even at extremely high temperatures.

As a start in understanding the kinetics and dynamics of these systems we have studied the ground state potential energy surfaces. These surfaces will be used to compute rate constants at high temperatures and for non-equilibrium conditions where experimental data are not available. The reactions studied here are also important at lower temperatures in hydrocarbon combustion as the Zeldovich mechanism for conversion of air  $\text{N}_2$  to  $\text{NO}_x$  [7].

A semi-quantitative study of the potential energy surfaces for the  $\text{N} + \text{O}_2 \rightarrow \text{NO} + \text{O}$  reaction has been carried out by Das and Benioff[8] using MCSCF and limited CI calculations. The current study includes more extensive electron correlation and uses a much more extensive basis set than in Ref. 8. The  $\text{O} + \text{N}_2$  reaction has also been discussed by Jaffe [3] using a phenomenological collision theory approach, but there have been no previous ab initio studies of the  $\text{O} + \text{N}_2$  reaction.

Section II discusses qualitative features of the reactions studied here. Section III describes the basis sets and computational method, while Section IV discusses the features of the computed potential surfaces. Finally, Section V presents the conclusions.

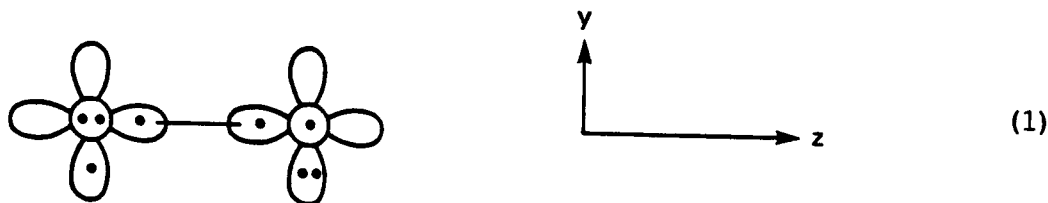
## II. Qualitative Features of the Reactions

First we consider the  $\text{N} + \text{O}_2 \rightarrow \text{NO} + \text{O}$  reaction. In  $C_\infty$  symmetry, which is appropriate for the description of the NOO potential energy surface, the ground state reactants  $\text{N} + \text{O}_2$  have  $^4\text{A}''$  and  $^2\text{A}''$  symmetry, respectively (without considering spin-orbit coupling). Thus,  $\text{N}(^4\text{S})$  and  $\text{O}_2(^3\Sigma_g^-)$  collisions can occur on  $^6\text{A}'$ ,  $^4\text{A}'$ , and  $^2\text{A}'$  potential energy surfaces with statistical weights of 6/12, 4/12, and 2/12, respectively. Similarly, the ground electronic state products have  $^2\text{A}'$  and  $^2\text{A}''$  ( $\text{NO } X^2\Pi$ ) and  $^3\text{A}'$  and  $^3\text{A}''$  ( $\text{O } ^3\text{P}$ ) symmetries. Thus, two sets of  $^4\text{A}'$ ,



$^4A''$ ,  $^2A'$ , and  $^2A''$  potential surfaces lead to the lowest product asymptote. Only the lowest  $^4A'$  and  $^2A'$  potential energy surfaces connect the lowest reactant and product asymptotes and only they are considered further in this work.

In a localized orbital description the ground state of the  $O_2$  molecule is represented as:

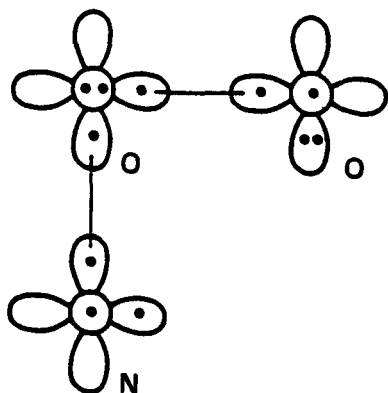


As discussed elsewhere[9] there is a second equivalent structure and resonance interactions between these two structures result in delocalization of the doubly-occupied  $\pi$  orbitals, so that the  $\pi_x$  and  $\pi_y$  orbitals are equivalent, leading to a  $^3\Sigma_g^-$  ground state with the valence configuration (in terms of real orbitals with the atoms lying on the  $z$  axis):

$$2\sigma_g^2 2\sigma_u^2 3\sigma_g^2 1\pi_{xu}^2 1\pi_{xg}^1 1\pi_{yu}^2 1\pi_{yg}^1 \quad (2)$$

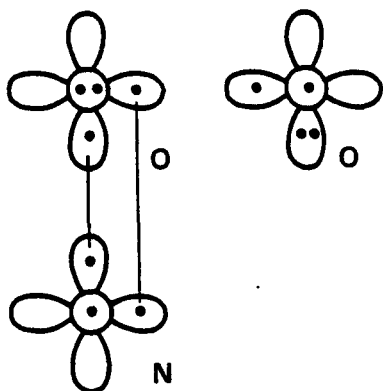
Here the  $2\sigma_g$  and  $2\sigma_u$  orbitals, which are not shown in (1), are derived from the  $2s$  orbitals. The remaining orbitals, which are shown in (1), are the  $3\sigma_g$  orbital which is the  $OO\sigma$  bonding orbital(derived from atomic  $2p\sigma$ ), and the  $\pi$  orbitals, which are derived from atomic  $2p_x$  and  $2p_y$ . First consider bringing up a hydrogen atom to (1) to form the ground  $^2A''$  state of  $HO_2$ . Since H- $O_2$  bond formation requires localization of the  $\pi$  orbitals as in (1), the HO bond energy is partially cancelled by loss of  $\pi$  bonding for  $O_2$  and there is the possibility of a barrier to H atom addition. POL-CI calculations[9] give a small barrier of 0.4 kcal/mole, although it was predicted that a more complete calculation would lead to no barrier. From (1) it is clear that the optimal angle of approach will involve  $\theta_{HOO}$  greater than  $90^\circ$ , since the bond pair formed between the H1s and the in plane singly-occupied  $O2p$  orbital in (1) must remain orthogonal to the doubly-occupied in-plane  $O2p$  orbital on the other O atom.

Bringing up a  $^4S$  N atom to  $O_2$  leads to the asymmetric NOO species shown in (3):



(3)

As for  $\text{H} + \text{O}_2$  the angle of approach will be greater than  $90^\circ$ . However, the  $\text{N} + \text{O}_2$  reaction is expected to have a larger entrance channel barrier than the  $\text{H} + \text{O}_2$  reaction because, upon bond formation, there is a loss of exchange interactions for the high-spin N atom in addition to the loss of  $\pi$  bonding for the  $\text{O}_2$  molecule. In addition to the two sigma bonds shown in (3), the two singly-occupied  $2p_x$  orbitals may be either singlet or triplet paired leading to  $^2\text{A}'$  and  $^4\text{A}'$  surfaces, respectively. The singlet pairing of these orbitals is energetically favored leading to a smaller barrier height for the  $^2\text{A}'$  surface as compared to the  $^4\text{A}'$  surface. Since the  $\text{N} + \text{O}_2$  reaction is exoergic by 32 kcal/mole, we expect an early barrier similar in electronic structure to  $\text{N} + \text{O}_2$  for the lowest  $^2\text{A}'$  and  $^4\text{A}'$  potential energy surfaces. Moving along the reaction coordinate,  $r_{\text{NO}}$  decreases and  $r_{\text{OO}}$  increases leading to the breaking of the  $\text{OO}\sigma$  bond and simultaneous formation of the in plane  $\pi$  bond of the product NO molecule as shown in (4).

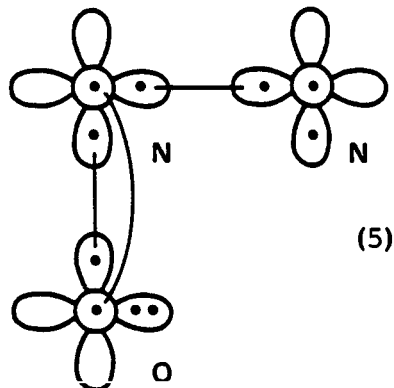


(4)

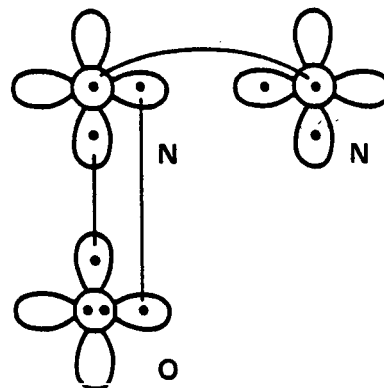
Because of the energetic nature of the reaction, we do not expect the asymmetric NOO to be a stable species, but rather we expect and find( see section IV) that the energy decreases monotonically moving along the reaction coordinate from the entrance channel saddle point to products.

Next we consider the  $O + N_2 \rightarrow NO + N$  reaction. Because this reaction is endoergic by 75 kcal/mole any barrier is expected to resemble  $NO + N$ . Thus, in the following discussion we consider the reaction from the reverse direction, and in fact the calculations have focused largely on the  $NO + N$  channel.

Combining the  $N\ ^4S$  state with the two components of the  $^2\Pi$  state of  $NO$  leads to  $^5A'$ ,  $^5A''$ ,  $^3A'$ , and  $^3A''$  surfaces in  $C_s$  symmetry. However,  $O^3P + N_2\ ^1\Sigma_g^+$  results in only  $^3A'$  and  $^3A''$  surfaces. In the present study only the latter two surfaces which connect ground state reactants and ground state products are considered. The electronic structures of the  $NO + N$  asymptote for the  $^3A''$  and  $^3A'$  surfaces are shown in (5) and (6), respectively.



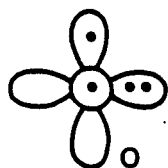
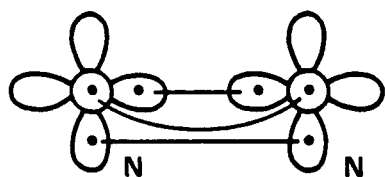
(5)



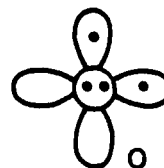
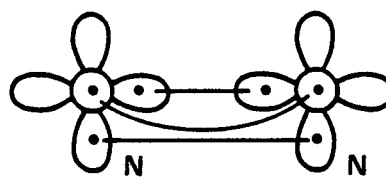
(6)

Here one sees that on the  $^3A''$  surface an initial  $NN\sigma$  bond forms as  $N$  and  $NO$  approach, while an initial  $NN\pi$  bond forms on the  $^3A'$  surface. Since  $\sigma$  overlaps are larger than  $\pi$  overlaps, the  $^3A''$  surface will have a smaller barrier than the  $^3A'$  surface. In fact one expects and finds (see section IV) that the  $^3A''$  surface has essentially no barrier while the  $^3A'$  surface has a significant one. As in the  $N + O_2$  case, the entrance channel barriers for these reactions result from the loss of exchange interactions for the high-spin  $N(^4S)$  atom as well as localization of the  $NO\ \pi$  orbitals.

The electronic structures for  $N_2 + O$  on the  $^3A''$  and  $^3A'$  surfaces are shown in (7) and (8), respectively. Here it is seen that product formation requires breaking  $NO\ \sigma$  and  $\pi$  bonds with simultaneous formation of two  $NN\ \pi$  bonds for the  $^3A''$  surface, while  $NO\ \pi$  and  $\sigma$  bonds are broken with simultaneous formation of an  $NN\ \sigma$  and  $\pi$  bond for the  $^3A'$  surface. More detailed descriptions of the changes in the bonding occurring during these reactions are given in section IV.



(7)



(8)

### III. Computational Details

Two different N and O basis sets were used. In both cases the sp basis sets were a [5s3p] segmented contraction of the van Duijneveldt (11s6p) primitive set[10]. The inner nine primitive functions were contracted (63) based on the 1s orbital, while the outer five s functions were contracted (311) based on the 2s orbital. (Note that this contraction uses three functions twice.) The first basis set was augmented by two sets of primitive 3d functions on each atom. The exponents were obtained by optimizing the scale factor for a two term GTO fit[11] to a 3d Slater for the ground states of the atoms at the SDCI level. The resulting two term GTO was then used uncontracted. The exponents used were 1.62 and 0.49 for N and 2.27 and 0.68 for O. The second basis set used the same effective Slater exponent for the 3d functions but used a 3 term fit contracted (21). In addition a single set of 4f functions was added as a two term fit[11] to effective Slater exponents of 2.5 and 3.0 for N and O, respectively. The N and O basis sets are given in Tables I and II, respectively.

The calculations consisted of Complete Active Space SCF (CASSCF)[12] followed by multireference Contracted CI (CCI)[13] as described below. The N2s and O2s derived orbitals were inactive in the CASSCF and were not correlated in the CCI. Since the CCI uses only a limited set of reference configurations, the CCI energy is not invariant to a unitary transformation of the CASSCF orbitals among themselves. The CASSCF active orbitals are uniquely defined by a natural orbital transformation of the converged active orbitals, followed by a CASSCF CI in the natural orbital basis to define the important reference configurations. The multireference analog of Davidson's correction[14] was added to the CCI energy at each computed point. The correction used in the CCI is  $\Delta E (1 - C_0^2)/C_0^2$  which differs slightly from the original Davidson's correction which is  $\Delta E (1 - C_0^2)$ , where  $\Delta E$

is the CI energy minus the reference energy and  $C_0^2$  is the square of the coefficient of the reference configuration or the sum of the squares of the coefficients of the reference configurations in the multireference case. Calculations where Davidson's correction have been added are denoted as CCI + Q. The calculations were carried out using the MOLECULE[15]-SWEDEN[16] system of programs.

#### A. The $N + O_2 \rightarrow NO + O$ Reaction

The ground state configuration of the  $O_2$  molecule was given in (2). In addition to the SCF orbitals given in (2), the  $3\sigma_u$  orbital which introduces left-right correlation of the sigma bond pair is also included in the CASSCF calculations. The ground state of NO is  $^2\Pi$  the two components of which are:

$$3\sigma^2 4\sigma^2 5\sigma^2 1\pi_y^2 1\pi_x^2 2\pi_y^1 \quad (9)$$

and

$$3\sigma^2 4\sigma^2 5\sigma^2 1\pi_y^2 1\pi_x^2 2\pi_x^1 \quad (10)$$

Here the  $3\sigma$  and  $4\sigma$  orbitals are derived from the  $O2s$  and  $N2s$  levels, the  $5\sigma$  is an  $NO\sigma$  bond orbital, and the  $\pi$  orbitals are derived from the  $N2p\pi$  and  $O2p\pi$  levels. The CASSCF wave function also includes a  $6\sigma$  orbital which introduces left-right correlation of the  $NO\sigma$  bond pair. Note also that both the  $2\pi_x$  and  $2\pi_y$  orbitals are included to describe both components of the  $^2\Pi$  state. Combining the N atom and  $O_2$  molecule  $2p$  orbitals leads to an active space consisting of  $7a' - 12a'$  and  $1a'' - 3a''$ . (The first six  $a'$  orbitals here correspond to the  $1s$  and  $2s$  orbitals on O and N which are inactive.) The qualitative character of these orbitals for reactants, saddle point, and products is given in Table III. CASSCF calculations were carried out for the lowest  $^2A'$  and  $^4A'$  surfaces of the  $N + O_2$  system using the active space defined above with the restriction that there were 7 electrons in  $a'$  orbitals and 4 electrons in  $a''$  orbitals. These constraints lead to 2142 configurations for the  $^2A'$  and 1404 configurations for the  $^4A'$  state. Two different sets of multireference CCI calculations were carried out using the appropriate CASSCF orbitals. The larger set of reference configurations used includes the configurations needed to describe dissociation of both the NO and OO bonds and is therefore able to provide a consistent description over the entire potential surface. The reference configurations for the CCI calculations were:

$$\begin{pmatrix} 7a'^2 8a'^2 12a'^0 \\ 7a'^1 8a'^2 12a'^1 \\ 7a'^0 8a'^2 12a'^2 \end{pmatrix} \times \begin{pmatrix} 9a'^2 10a'^1 11a'^0 \\ 9a'^1 10a'^1 11a'^1 \\ 9a'^0 10a'^1 11a'^2 \end{pmatrix} \times \begin{pmatrix} 1a''^2 2a''^2 3a''^0 \\ 1a''^2 2a''^1 3a''^1 \\ 1a''^2 2a''^0 3a''^2 \end{pmatrix} \quad (11)$$

$$7a'^2 8a'^1 \times 9a'^2 10a'^1 11a'^1 \times 1a''^1 2a''^2 3a''^1 \quad (12)$$

This reference set includes all the configurations with CI coefficients greater than 0.05 in the CASSCF wave function for the  $^2A'$  state. Here the first 27 configurations given by (11) are important in the saddle point region, while the last configuration (12) is important in the  $N + O_2$  asymptotic region. This CCI calculation (denoted by ext. CCI) involves about three million configurations(uncontracted).

Calculations were also carried out with a smaller set of reference configurations consisting of the subset of the configurations above which have no electrons in the  $12a'$  orbital. The resulting CCI calculation (denoted by CCI) involves approximately one million configurations(uncontracted).

The CCI wavefunction is adequate to describe the reactants and entrance channel saddle point region of the surface, since in these regions the OO bond length is close to that of free  $O_2$ , and for this limited region of the surface it is not critically important to include configurations which are needed to break the O-O bond. An analogous CCI wavefunction would also be adequate to describe the product region of the surface. From Table III it is seen that for products,  $7a'$  and  $12a'$  describe an  $NO\pi$  bond, while  $9a'$  and  $11a'$  describe the  $NO\sigma$  bond pair. This change in orbital character is no problem for the ext. CCI calculation, since these two pairs are treated equivalently, but for the CCI calculation these two pairs would have to be interchanged to be consistent with the configurations given in (11) and (12). However, CCI calculations were not carried out for the product region for this reaction.

While the CCI wavefunction is adequate in the reactants and products regions, it is clearly not adequate in the intermediate region between the entrance channel saddle point and the products region where both the OO and NO bonds are elon-

gated. In addition, as discussed in section IV, the entrance channel barrier height obtained for CCI is 1.7 kcal/mole higher than for the ext. CCI defined above. In spite of this, it is expected and found that the saddle point location obtained with the CCI is not changed by the ext. CCI and other features of the CCI surface are expected to be reasonably accurate over the limited region of the surface for which this wavefunction is valid. As also discussed in Section IV, calculations were carried out along an approximate minimum energy path using the ext. CCI. The entrance channel saddle point location was determined using the CCI with the [5s3p2d] basis set and subsequent calculations were carried out using the ext. CCI with the [5s3p2d] basis set and the CCI with a larger [5s3p2d1f] basis set as described above. The barrier height was estimated by assuming that the effects of expanding the reference space in the CCI and the effects of expanding the basis set are additive.

For the  $^4A'$  surface CCI and ext. CCI calculations were carried out, where the reference configurations consisted of the subset of the configurations used for the  $^2A'$  surface which contained three or more open shells.

#### B. The $O + N_2 \rightarrow NO + N$ Reaction

Here the calculations concentrated on the  $NO + N$  channel. The ground state configuration for the two components of the  $^2\Pi$  state of NO is given in (9) and (10). The ground state configuration of  $N_2$  is:

$$2\sigma_g^2 2\sigma_u^2 3\sigma_g^2 1\pi_{xu}^2 1\pi_{yu}^2 \quad (13).$$

In addition to the SCF orbitals given above the CASSCF calculation also includes the  $3\sigma_u$  and  $1\pi_g$  orbitals which are correlating orbitals for the  $\sigma$  and  $\pi$  bonds, respectively. Combining the  $^4S$  N atom with NO  $^2\Pi$  leads to a  $^3A''$  surface for (9) and a  $^3A'$  surface for (10). The CASSCF active space for these surfaces consists of  $7a' - 12a'$  and  $1a'' - 3a''$ . The qualitative character of the CASSCF orbitals for reactants, saddle point, and products regions of the surface is given in Tables IV and V for the  $^3A''$  and  $^3A'$  states, respectively. CASSCF calculations were carried out for the  $^3A''$  surface with the constraint that there were 7 electrons in  $a'$  orbitals and 3 electrons in  $a''$  orbitals, which leads to 2652 configurations. CASSCF calculations were also carried out for the  $^3A'$  surface with the constraint that there were 6 electrons in  $a'$  orbitals and 4 electrons in  $a''$  orbitals, which leads to 2331

configurations.

CCI calculations were also carried out for both surfaces for the N + NO asymptotic regions and for the saddle point region. As in the N + O<sub>2</sub> study, the 12a' orbital was not included in the active space for the CCI calculations, since for the limited region of the surface studied it was not necessary to include configurations which dissociate the NOσ bond. The reference configurations for the CCI calculations, which again include all configurations with CI coefficients greater than 0.05 in the CASSCF wave function, were:

$$7a'^2 8a'^2 \times \begin{pmatrix} 9a'^2 10a'^1 11a'^0 \\ 9a'^1 10a'^1 11a'^1 \\ 9a'^0 10a'^1 11a'^2 \end{pmatrix} \times \begin{pmatrix} 1a''^2 2a''^1 3a''^0 \\ 1a''^1 2a''^1 3a''^1 \\ 1a''^0 2a''^1 3a''^2 \end{pmatrix} \quad (14)$$

$$7a'^2 8a'^1 \times 9a'^2 10a'^1 11a'^1 \times 1a''^1 2a''^1 3a''^1 \quad (15)$$

for the <sup>3</sup>A'' surface, and :

$$7a'^2 \times \begin{pmatrix} 8a'^2 9a'^1 10a'^1 11a'^0 \\ 8a'^1 9a'^1 10a'^1 11a'^1 \\ 8a'^0 9a'^1 10a'^1 11a'^2 \end{pmatrix} \times \begin{pmatrix} 1a''^2 2a''^2 3a''^0 \\ 1a''^2 2a''^1 3a''^1 \\ 1a''^2 2a''^0 3a''^2 \end{pmatrix} \quad (16)$$

$$7a'^2 \times 8a'^1 9a'^1 10a'^1 11a'^1 \times 1a''^1 2a''^2 3a''^1 \quad (17)$$

for the <sup>3</sup>A' surface. The CCI calculations in each case involved slightly more than one million configurations(uncontracted).

For the <sup>3</sup>A'' surface, CCI calculations were also carried out for the N<sub>2</sub> + O asymptotic regions. From Table IV it is seen that for the products, 7a' and 12a'



describe an  $NN\pi$  bond, while  $9a'$  and  $11a'$  describe the  $NN\sigma$  bond pair. This change in orbital character requires an interchange of these bond pairs for the product region in order to be consistent with the configurations given in (14) and (15). However, with this change the reactant and product regions are treated equivalently. One point was also computed for  $N + N + O$  at large internuclear separation using a high spin supermolecule calculation. This result in conjunction with the calculations for the asymptotic regions enables computation of the  $D_e$  of NO and  $N_2$  in a supermolecule calculation. The  $D_e$  of NO obtained here was used in conjunction with the  $D_e$  of  $O_2$  obtained in an analogous fashion for the  $N + O_2$  surface to compute the heat of reaction for the  $N + O_2$  reaction.

#### IV. Results and Discussion.

The computed energies for the  $N + O_2$   $^2A'$  and  $^4A'$  surfaces and the  $O + N_2$   $^3A'$  and  $^3A''$  surfaces are given in the appendix. For the  $N + O_2$   $^2A'$  surface CASSCF calculations were carried out at enough points to define the global potential energy surface which is given in Fig. 1. As indicated earlier, the CCI calculations were carried out for the reactants and entrance channel saddle point regions, while the ext. CCI calculations were carried out along the minimum energy path defined by the CASSCF and CCI surface. For the  $^4A'$  surface of  $N + O_2$ , CCI calculations were carried out for the saddle point region and one calculation was carried out at the saddle point determined in the CCI using the ext. CCI. For the  $N_2 + O$  reaction, CCI calculations were carried out for the reactant, saddle point, and product regions for the  $^3A''$  surface and for the NO + N asymptotic and saddle point regions for the  $^3A'$  surface. All of the above calculations were carried out with the [5s3p2d] basis set. CCI calculations were also carried out using the larger [5s3p2d1f] basis set for the saddle points and asymptotic ( $N + O_2$  and  $NO + N$ ) regions for all four surfaces.

##### A. The $O_2$ , NO, and $N_2$ Molecules

Spectroscopic constants for the  $O_2$ , NO, and  $N_2$  molecules were derived from supermolecule calculations for the  $N + O_2$ ,  $NO + N$ , and  $O + N_2$  limits using CCI with the smaller basis set. In addition, calculations were carried out for the above diatomic molecules using both basis sets. For the smaller basis set, the supermolecule calculations differ from the molecular calculations in that they have

the  $\sigma$  bond pair doubly-occupied in all reference configurations, while the molecular calculations include as reference configurations products of all excitations within the  $\sigma$ ,  $\pi_x$  and  $\pi_y$  spaces which have the correct molecular symmetry (equivalent to the larger set of reference configurations). Thus, these calculations test the effect of the restrictions made on the reference configurations in the smaller reference space CCI calculations. The calculations with the larger basis set in turn test the effect of 4f functions. In addition calculations were carried out for the diatomics with and without correlating the N2s and O2s derived orbitals in order to test the approximation made in the potential surface calculations of not correlating those orbitals. In each case,  $r_e$ ,  $\omega_e$ , and  $D_0$  were computed via a Dunham analysis of a quartic energy expansion. Thus, the computed  $\omega_e$  and  $D_0$  values include corrections for anharmonicity in the potential.

The results are summarized in Table VI. Looking first at the supermolecule CCI results we see that the computed  $r_e$  and  $\omega_e$  values are in excellent agreement with experiment[17], but the  $D_0$  values are consistently too small. The error in  $D_0$  comes from two major sources. The first is the restriction of leaving the diatomic  $\sigma$  bond pair doubly-occupied in all reference configurations. This leads to an error in the binding energy of  $O_2$  of 0.17 eV. The second source of error is the limited basis set. Here we see that the larger basis set increases the binding energy of  $O_2$  by 0.27 eV. At this level of calculation the errors in the computed  $D_0$  are 0.14, 0.05, and 0.16 eV for  $O_2$ , NO, and  $N_2$ , respectively. For  $O_2$  and  $N_2$  the effect of correlating the O2s and N2s electrons was also examined. Correlating these additional electrons decreases the  $D_0$  by 0.10 eV and 0.41 eV for  $O_2$  and  $N_2$ , respectively. The decrease in binding energy when the 2s shell is correlated probably results from size-consistency errors. However, it is clear that calculations with the 2s electrons not correlated lead to better results for the diatomics and thus this approximation is reasonable for the potential surface calculations. Table VI also compares results with the contracted CI to results without contraction (denoted by SDCI). The largest contraction error is 0.08 eV for the  $D_0$  of  $O_2$ . This result indicates that the CCI method works well for the systems studied here.

It may also be seen in Table VI that bond lengths and harmonic frequencies obtained at the CASSCF level are accurate but those calculations obtain a smaller

percentage of the binding energy than CASSCF/CCI. From these results we might expect that the geometries and force fields computed from the CASSCF/CCI potential surface will be accurate, but the CASSCF surfaces will have larger barriers than the CCI surfaces. What is actually found is that the CASSCF method gives reasonable geometries and force constants perpendicular to the reaction coordinate, but that the barrier location along the reaction coordinate is shifted for CCI compared to CASSCF. In addition the approximations of restricting the reference space in the supermolecule CCI calculations as well as the omission of 4f functions in the smaller basis set are expected to increase the barrier height since these constraints decrease the diatomic binding energies. These two effects were tested for the potential surface calculation as described above.

#### B. The $\text{N} + \text{O}_2 \rightarrow \text{NO} + \text{O}$ Reaction.

Fig. 1 shows a plot of the  $^2\text{A}'$  CASSCF surface for the  $\text{N} + \text{O}_2$  system. Along the minimum energy path connecting reactants and products this surface has two saddle points and one local minimum. The first saddle point is in the entrance channel as expected. In this region of the surface, the predominant interaction is between the  $\text{O}_2 1\pi_{yg}$  orbital and one of the in plane  $\text{N}2p$  orbitals leading ultimately to formation of an  $\text{NO}\sigma$  bond pair. In a simple valence bond picture one might expect an  $\text{NOO}$  angle of  $90^\circ$ , however repulsive interactions with the  $\text{O}_2 1\pi_{gu}$  orbital lead to a somewhat larger angle of about  $110^\circ$  for the entrance channel saddle point region. There is a significant barrier (best estimate about 10 kcal/mole) which arises from loss of exchange interactions for the high-spin  $^4\text{S}$  N atom as well as loss of resonance interactions in the  $\text{O}_2$  molecule due to the localization of the  $\pi$  electrons upon NO bond formation. Shortening the NO bond further leads to a bent asymmetric NOO species which is actually a very shallow minimum on the CASSCF surface. This species is unstable relative to  $\text{NO} + \text{O}$  and the second very low energy saddle point corresponds to transferring the  $\text{OO}\sigma$  bond pair to become a  $\pi$  bond for the product NO molecule. As discussed later the shallow minimum on the CASSCF surface disappears for the ext. CCI calculations, leading to a single saddle point in the entrance channel.

An insertion process to form symmetric  $\text{NO}_2$  was also considered but there appears to be a large energy barrier for this reaction and we conclude that formation

of transient symmetric  $\text{NO}_2$  would not proceed readily from  $^4\text{S N}$  plus  $\text{O}_2$ .

Table III gives the qualitative character of the orbitals for reactants, saddle point, and products. Here the  $7a'$  orbital corresponds to the  $\text{OO}\sigma$  bonding orbital and the  $8a'$  and  $1a''$  orbitals correspond to the  $1\pi_u$  orbitals of  $\text{O}_2$ . In the reactants and saddle point regions, these orbitals are not substantially changed from free  $\text{O}_2$ . There are two bonding interactions. The first involves the  $\text{O}_2 1\pi_{yg}$  orbital and one of the in plane  $\text{N}2p$  orbitals. The natural orbitals of this bond pair are the  $9a'$  and  $11a'$  orbitals, which correspond approximately to:  $\text{O}_2 1\pi_{yg} \pm \text{N}2p$ , respectively. Proceeding to products this bond pair localizes to become the  $\text{NO}\sigma$  bond. The other in plane  $\text{N}2p$  orbital is the  $10a'$  orbital which remains essentially atomic like in the saddle point region. However, proceeding to products the  $7a'$  and  $10a'$  orbitals spin recouple to form the  $\text{NO} 1\pi_y$  bond pair and a  $2p$  orbital on the product oxygen atom. The second bond in the saddle point region involves the  $\text{O}_2 1\pi_{xg}$  and the  $\text{N}2p_x$  orbitals. The natural orbitals of this bond pair are the  $2a''$  and  $3a''$  orbitals, which correspond approximately to:  $\text{O}_2 1\pi_{xg} \pm \text{N}2p_x$ , respectively. The  $a''$  pair is only weakly bonding (biradical like) and relocates to the singly-occupied  $\text{NO} 2\pi_x$  and  $\text{O} 2p_x$  orbitals for products. At the same time that these changes are occurring the  $8a'$  orbital localizes on the product  $\text{O}$  atom and the  $1a''$  orbital localizes on the  $\text{NO}$  to become the  $1\pi_x$  orbital.

Given the weak coupling of the  $a''$  pair in the saddle point region the  $^4A'$  CASSCF natural orbitals are very similar to those of the  $^2A'$  surface. Loss of the  $a''$  bonding interactions leads to a barrier for the  $^4A''$  surface about 8 kcal/mole higher than the doublet surface. At low temperatures the rate constant will be controlled primarily by the  $^2A'$  surface, owing to the lower barrier to reaction, but at higher temperatures both the  $^2A'$  and  $^4A'$  surfaces will be important with the  $^4A'$  surface having twice the statistical weight of the  $^2A'$  surface.

In order to locate the saddle points for the  $^2A'$  and  $^4A'$  surfaces, grids of points were computed in  $r_{\text{NO}}$  and  $r_{\text{OO}}$  for an  $\text{NOO}$  angle of  $110^\circ$  using the smaller basis set at the CCI level. This angle was estimated from preliminary CASSCF calculations; it was subsequently varied about the saddle point obtained for a fixed angle of  $110^\circ$  and was found to be very close to the optimal value. The saddle point on the  $r_{\text{NO}}$  and  $r_{\text{OO}}$  grid was obtained from a fit of the energies to a quadratic polynomial of

the form:

$$E(r_{NO}, r_{OO}) = c_1 + c_2 r_{NO} + c_3 r_{OO} + c_4 r_{NO} r_{OO} + c_5 r_{NO}^2 + c_6 r_{OO}^2 \quad (18)$$

To this polynomial was added a quadratic term in the NOO angle and the vibrational frequencies at the saddle point were obtained from this energy expression using the conventional F and G matrix method[18]. Calculations were also carried out using the larger basis set at the CCI level and using the smaller basis set at the ext. CCI level. The results are given in Table VII. Here for the  $^2A'$  surface it is seen that at the CCI + Q level with the smaller basis set the computed barrier is 13.4 kcal/mole. The larger basis set reduces the barrier by 1.5 kcal/mole, while the ext. CCI reduces the barrier by 1.7 kcal/mole. Combining these two effects leads to 10.2 kcal/mole as our best estimate of the barrier. From Table VII it is seen that the saddle point location with the ext. CCI is very similar to the saddle point location obtained with the CCI. Table VII also shows the saddle point vibrational frequencies and computed zero point correction. The zero point correction is +0.44 kcal/mole leading to an effective barrier of 10.6 kcal/mole. This number may be compared to an experimental activation energy of 6-8 kcal/mole[6,19] which suggests that the computed barrier is too large by at least 2-3 kcal/mole. At least part of this error results from basis set effects, since for the  $O + H_2$  reaction, addition of a third d, a second f, and a g function to the O basis set used in these studies in conjunction with improvements in the H basis set lowered the barrier height by more than 1.0 kcal/mole[20]. There may also be some remaining differential effect due to higher excitations. The Davidson's correction at the saddle point geometry is 0.023 hartree, while the differential Davidson's correction between reactants and saddle point is 2.9 kcal/mole for the ext. CCI. These results indicate that higher excitations are still significant for the highest level of correlation treatment considered here and may account for a large part of the remaining error in the barrier height. The computed saddle point geometry has an NOO angle of  $115^\circ$ . The bending potential about the saddle point geometry is shown in Fig. 2.

Table VII also shows the results for the CASSCF calculations. Here it is seen that the barrier height is about 8 kcal/mole larger than the best CCI result using the same basis set. Also, the saddle point is shifted somewhat toward shorter  $r_{NO}$ . These results are consistent with the conclusion, deduced from studies of the  $O +$

$\text{H}_2$ [21] and  $\text{OH} + \text{H}_2$ [22] reactions, that MCSCF wave functions give consistently high barriers. Table VII also shows the calculated exoergicity for the reaction. Here  $\text{CCI} + \text{Q}$  gives 30.9 kcal/mole while CASSCF gives 35.0 kcal/mole, compared to the experimental value of 32 kcal/mole[17].

Table VIII shows computed energies along the minimum energy path for the  $\text{N} + \text{O}_2$  reaction on the CASSCF, CCI, and ext. CCI  $^2\text{A}'$  surfaces. These minimum energy paths were obtained from the CASSCF surface by interpolation on the rectangular grid of CASSCF and CCI energies computed for an angle of  $110^\circ$ . In the intermediate region this corresponds to a rotated Morse oscillator description with a pivot point at  $r_{\text{NO}} = 2.9$  and  $r_{\text{OO}} = 3.1$ . For  $r_{\text{NO}}$  greater than 2.9 and  $r_{\text{OO}}$  greater than 3.1 the reaction coordinate is approximately  $r_{\text{OO}}$  and  $r_{\text{NO}}$ , respectively. One interesting feature of Table VIII is that the shallow minimum corresponding to an asymmetric NOO structure on the CASSCF surface disappears at the ext. CCI level.

A similar treatment was carried out for the  $^4\text{A}'$  surface. The resulting saddle point geometry is given in Table VII, while the bending potential is shown in Fig. 2 and the minimum energy paths at both the CASSCF and  $\text{CCI} + \text{Q}$  level are given in Table IX. Additional calculations were carried out at the saddle point geometry which was obtained with the smaller basis set and smaller set of reference configurations using i) CCI with the larger basis set and ii) ext. CCI with the smaller basis set. These results are also given in Table VII. Here it is seen that the larger basis set lowers the barrier by 1.5 kcal/mole, while the ext. CCI lowers the barrier by 1.1 kcal/mole. Combining these two effects leads to 18.0 kcal/mole as the best estimate of the barrier, although based on the  $^2\text{A}'$  surface we expect that this barrier is still too large by 2-3 kcal/mole. Other than the larger barrier height, the general features of this surface are similar to those of the  $^2\text{A}'$  surface.

### C. The $\text{O} + \text{N}_2 \rightarrow \text{NO} + \text{N}$ Reaction.

Calculations were carried out for both the  $^3\text{A}''$  and  $^3\text{A}'$  surfaces. The calculations focused primarily on the  $\text{NO} + \text{N}$  channel. Table IV shows the qualitative nature of the orbitals for the  $^3\text{A}''$  surface of the  $\text{N} + \text{NO}$  reaction for reactants, saddle point, and products. Here the  $7\text{a}'$  orbital corresponds to the  $\text{NO}\sigma$  bond pair, the  $8\text{a}'$  and  $1\text{a}''$  orbitals correspond to the two components of the  $\text{NO}1\pi$  orbital. There is one

bond pair formed between the  $\text{NO}2\pi$  orbital and one of the in plane  $\text{N}2p$  orbitals. The natural orbitals of this bond pair are the  $9a'$  and  $11a'$  orbitals which correspond approximately to:  $\text{NO}2\pi_y \pm \text{N}2p$ , respectively. This bond pair becomes the  $\text{NN}\sigma$  bond pair for the products. The remaining orbitals are the  $2a''$  and the  $10a'$  which are atomic  $\text{N}2p$  like. To go to the  $\text{N}_2 + \text{O}$  products requires spin recoupling of the  $7a'$  and  $10a'$  orbitals to form one  $\pi$  bond with simultaneous spin recoupling of the  $1a''$  and  $2a''$  orbitals to form the other  $\pi$  bond of  $\text{N}_2$ .

Table V shows the qualitative nature of the orbitals for the  ${}^3A'$  surface for the reactants, saddle point, and products regions. Here the  $7a'$  orbital corresponds to the  $\text{NO} \sigma$  bond pair, and the  $8a'$  and  $1a''$  orbitals correspond to the two components of the  $\text{NO}1\pi$  orbital. The  $11a'$  orbital is a correlating orbital for the in plane  $\text{NO}\pi$  orbital, and the  $9a'$  and  $10a'$  orbitals are  $\text{N}2p$  orbitals. There is one bond pair formed between the  $\text{NO}2\pi$  orbital and the  $\text{N}2p_x$  orbital. The natural orbitals of this bond pair are the  $2a''$  and  $3a''$  orbitals which correspond approximately to:  $\text{NO}2\pi_x \pm \text{N}2p_x$ , respectively. This bond pair becomes an  $\text{NN}\pi$  bond pair for the products. To go to the  $\text{N}_2 + \text{O}$  limit requires spin recoupling of the  $8a'$  and  $9a'$  orbitals to form the  $\text{NN}\sigma$  bond, with simultaneous spin recoupling of the  $7a'$  and  $10a'$  orbitals to form the other  $\text{NN}\pi$  bond.

The  ${}^3A''$  surface has a very small barrier which occurs for large  $r_{\text{NN}}$ , while the  ${}^3A'$  surface has a substantial barrier which occurs for smaller  $r_{\text{NN}}$ . For both surfaces, grids of points in  $r_{\text{NN}}$  and  $r_{\text{NO}}$  were computed for a fixed  $\theta_{\text{NNO}}$  of  $110^\circ$ .  $\theta_{\text{NNO}}$  was then varied about the approximate saddle point position and the resulting bending curves are shown in Fig. 3.

Table X summarizes the computed potential surface properties for the  $\text{O} + \text{N}_2$  reaction. The CCI results with the larger basis set yielded computed barriers of 0.5 kcal/mole for  ${}^3A'$  and 14.4 kcal/mole for  ${}^3A''$ . In both cases the zero point corrections are positive leading to corrected barrier heights of 1.0 kcal/mole and 14.7 kcal/mole, respectively. It is likely that further improvement in the calculation would lead to no barrier for the  ${}^3A''$  surface. The computed endoergicity for this reaction is 77.0 kcal/mole at the CCI + Q level and 80.6 kcal/mole at the CASSCF level compared to an experimental value of 75 kcal/mole[17].

Tables XI and XII show the computed minimum energy paths for both CASSCF

and CCI + Q calculations of the  $^3A''$  and  $^3A'$  surfaces, respectively. These results are plotted in Fig. 4. As noted for  $N + O_2$ , the CASSCF calculation leads to too large a barrier height and shifted saddle point locations relative to the CCI + Q surface. As discussed earlier the differences between the  $^3A'$  and  $^3A''$  surfaces result from the different strengths of the initial N-NO bond. For the  $^3A'$  surface the  $NN\pi$  bond is too weak to compensate for loss of exchange interactions for the high-spin  $N(^4S)$  atom. Thus, the saddle point occurs for shorter atom-diatom distances and has a higher barrier for the  $^3A'$  surface. From these results we expect that, even at fairly high temperatures, the reverse reaction i.e.  $N + NO \rightarrow N_2 + O$  will occur almost entirely on the  $^3A''$  surface.

## V. Conclusions.

CASSCF/CCI calculations have been carried out for the  $^2A'$  and  $^4A'$  surfaces for the  $N + O_2 \rightarrow NO + O$  reaction and for the  $^3A'$  and  $^3A''$  surfaces for the  $O + N_2 \rightarrow NO + N$  reaction.

The  $N + O_2$  reaction is exoergic by 32 kcal/mole, which leads to an early barrier of 10.2 kcal/mole for the  $^2A'$  surface. The computed barrier height is about 3 kcal/mole larger than the experimental activation energy of 7-8 kcal/mole, after consideration of zero point energy differences. The  $^4A'$  surface has a larger barrier, 18.0 kcal/mole.

The  $O + N_2$  reaction is endoergic by 75 kcal/mole and is computed to have approximately a 1.0 kcal/mole additional energy barrier (resembling  $NO + N$ ). However, considering the limitations of the calculations there is probably no additional barrier. The barrier region to the reverse reaction was considered in detail. Combining  $N(^4S)$  with the two components of the  $^2\Pi$  ground state of NO leads to  $^3A'$  and  $^3A''$  states. The potential surfaces for these two states differ significantly, with the  $^3A''$  surface being characterized by a large atom-diatom distance and very small barrier (0.5 kcal/mole), while the  $^3A'$  surface has a smaller atom-diatom distance and a large barrier (14.4 kcal/mole). These differences are related to the relative strengths of the initially formed bonds. The  $^3A''$  surface initially forms an  $NN\sigma$  bond, while the  $^3A'$  surface initially forms a weaker  $NN\pi$  bond. The stronger  $NN\sigma$  bond in the case of the  $^3A''$  surface is better able to compensate for loss of exchange interactions for the high-spin  $N(^4S)$  atom as compared to the weaker  $NN\pi$  bond in



the case of the  $^3A'$  surface. These qualitative differences imply that reaction of N and NO would occur primarily on the  $^3A''$  surface.

## ACKNOWLEDGMENTS

S.P. Walch was supported by a NASA grant(NCC2-296).

## References

1. E.E. Whiting, J.O. Arnold, W.A. Page, and R.M. Reynolds, *J. Quant. Spectroscopy and Radiative Transfer*, **13**, 837(1973).
2. C. Park, in "Thermal Design of Aeroassisted Orbital Transfer Vehicles", edited by H.F. Nelson, Vol. 96 of Progress in Astronautics and Aeronautics, 1985, pp. 511-537.
3. R.L. Jaffe, "Rate Constants for Chemical Reactions in High-Temperature Non-Equilibrium Air", paper no. AIAA-85-1038, 20th Thermophysics Conference, Williamsburg, Va., June 19-21, 1985.
4. J.R. Stallcop and H. Partridge, *Phys. Rev. A*, **32**, 639(1985).
5. H. Partridge and S.R. Langhoff, to be published.
6. D.L. Baulch, D.D. Drysdale, D.G. Horn, and A.C. Lloyd, "Evaluated Kinetic Data for High Temperature Reactions, Vol 2., Homogeneous Gas Phase Reactions of the  $H_2-N_2-O_2$  System", Chemical Rubber Co. Press, Cleveland, 1973.
7. J. Blauwens, B. Smets, and J. Peeters, Sixteenth Symposium (International) on Combustion, p. 1055, The Combustion Institute, 1976, and references therein.
8. G. Das and P.A. Benioff, *Chem. Phys. Lett.*, **75**, 519(1980).
9. T.H. Dunning, Jr., S.P. Walch, and M.M. Goodgame, *J. Chem. Phys.*, **74**, 3482(1981).
10. F.B. van Duijneveldt, IBM Technical Research Report No. RJ945 (1971).
11. R.F. Stewart, *J. Chem. Phys.*, **52**, 431(1970).
12. P.E.M. Siegbahn, A. Heiberg, B. Roos, and B. Levy, *Physica Scripta*, **21**, 323(1980).
13. P.E.M. Siegbahn, *Int. J. of Quantum Chem.*, **23**, 1869(1983).
14. S.R. Langhoff and E.R. Davidson, *Int. J. of Quantum Chem.*, **8**, 61(1974).
15. J. Almlöf, MOLECULE, a Gaussian integral program.
16. P.E.M. Siegbahn, C.W. Bauschlicher, Jr., B. Roos, A. Heiberg, P.R. Taylor, and J. Almlöf, SWEDEN, A vectorized SCF MCSCF direct CI.

17. K.P. Huber and G. Herzberg, "Molecular Spectra and Molecular Structure", (Van Nostrand Reinhold, New York, 1979.)
18. E.B. Wilson, Jr., J.C. Decius, and P.C. Cross, Molecular Vibrations: The Theory of Infrared and Raman Vibrational Spectra, McGraw-Hill, New York, 1955.
19. R.R. Herm, B.J. Sullivan, and M.E. Whitson, Jr., J. Chem. Phys., **79**, 2221(1983).
20. S.P. Walch, J. Chem. Phys., to be published.
21. S.P. Walch, T.H. Dunning, Jr., R.C. Raffanetti, and F.W. Bobrowicz, J. Chem. Phys., **72**, 406(1980).
22. S.P. Walch and T.H. Dunning, Jr., J. Chem. Phys., **72**, 1303(1980).

Table I. Basis Sets for Nitrogen.

N [5s3p] valence basis		
function	s	p
1	22800.200(0.00022)	49.3707(0.00553)
2	3413.4500(0.00172)	11.3801(0.03791)
3	776.38300(0.00891)	3.43690(0.14903)
4	219.96600(0.03602)	<u>1.18210(0.34890)</u>
5	71.795200(0.11551)	<u>0.41746(1.00000)</u>
6	<u>25.817500(0.27756)</u>	<u>0.14285(1.00000)</u>
7	9.9295400(0.42314)	
8	3.9484300(0.27113)	
9	<u>1.1108500(0.02441)</u>	
7	9.9295400(-.14304)	
8	3.9484300(-.14193)	
9	<u>1.1108500(0.24422)</u>	
10	<u>0.436520(1.00000)</u>	
11	0.160920(1.00000)	

[2d1f] polarization basis		
function	d	f
1	3.0620(0.16866)	1.254(0.47694)
2	<u>0.9600(0.58480)</u>	0.429(0.65874)
3	0.3740(1.00000)	

Table II. Basis Sets for Oxygen.

O [5s3p] valence basis		
function	s	p
1	31195.560(0.00021)	64.7719(0.00584)
2	4669.3800(0.00163)	14.9727(0.04058)
3	1062.2600(0.00845)	4.55440(0.15754)
4	301.42600(0.03419)	<u>1.56370(0.35300)</u>
5	98.515300(0.11031)	<u>0.54107(1.00000)</u>
6	<u>35.460900(0.26949)</u>	0.17776(1.00000)
7	13.617900(0.42355)	
8	5.3862000(0.28304)	
9	<u>1.5387000(0.02748)</u>	
7	13.617900(-.14601)	
8	5.3862000(-.14788)	
9	<u>1.5387000(0.23867)</u>	
10	<u>0.605500(1.00000)</u>	
11	<u>0.220500(1.00000)</u>	

[2d1f] polarization basis		
function	d	f
1	4.2770(0.16866)	1.806(0.47694)
2	<u>1.3410(0.58480)</u>	0.618(0.65874)
3	<u>0.5220(1.00000)</u>	

Table III. Qualitative Character of the CASSCF Orbitals for  
 $\text{N} + \text{O}_2 \rightarrow \text{NO} + \text{O}$ ,  $^2,4\text{A}'$  Surface

orbital	reactants	saddle point	products
7a'	$\text{O}_2 3\sigma_g$	$\text{O}_2 3\sigma_g$	$\text{NO} 1\pi_y$
8a'	$\text{O}_2 1\pi_{yu}$	$\text{O}_2 1\pi_{yu}$	$\text{O}_2 p_y$
9a'	$\text{O}_2 1\pi_{yg}$	$\text{O}_2 1\pi_{yg} + \text{N} 2p_y$	$\text{NO} 5\sigma$
10a'	$\text{N} 2p_z$	$\text{N} 2p_z$	$\text{O}_2 p_z$
11a'	$\text{N} 2p_y$	$\text{O}_2 1\pi_{yg} - \text{N} 2p_y$	$\text{NO} 6\sigma$
12a'	$\text{O}_2 3\sigma_u$	$\text{O}_2 3\sigma_u$	$\text{NO} 2\pi_y$
1a''	$\text{O}_2 1\pi_{xu}$	$\text{O}_2 1\pi_{xu}$	$\text{NO} 1\pi_x$
2a''	$\text{O}_2 1\pi_{xg}$	$\text{O}_2 1\pi_{xg} + \text{N} 2p_x$	$\text{NO} 2\pi_x + \text{O}_2 p_x$
3a''	$\text{N} 2p_x$	$\text{O}_2 1\pi_{xg} - \text{N} 2p_x$	$\text{NO} 2\pi_x - \text{O}_2 p_x$

Table IV. Qualitative Character of the CASSCF Orbitals for  
 $\text{NO} + \text{N} \rightarrow \text{N}_2 + \text{O}, {}^3\text{A}''$  Surface

orbital	reactants	saddle point	products
7a'	NO5 $\sigma$	NO5 $\sigma$	N <sub>2</sub> 1 $\pi_{yu}$
8a'	NO1 $\pi_y$	NO1 $\pi_y$	O2p <sub>z</sub>
9a'	NO2 $\pi_y$	NO2 $\pi_y$ + N2p <sub>z</sub>	N <sub>2</sub> 3 $\sigma_g$
10a'	N2p <sub>y</sub>	N2p <sub>y</sub>	O2p <sub>y</sub>
11a'	N2p <sub>z</sub>	NO2 $\pi_y$ - N2p <sub>z</sub>	N <sub>2</sub> 3 $\sigma_u$
12a'	NO6 $\sigma$	NO6 $\sigma$	N <sub>2</sub> 1 $\pi_{yg}$
1a''	NO1 $\pi_x$	NO1 $\pi_x$	N <sub>2</sub> 1 $\pi_{xu}$
2a''	N2p <sub>x</sub>	N2p <sub>x</sub>	O2p <sub>x</sub>
3a''	NO2 $\pi_x$	NO2 $\pi_x$	N <sub>2</sub> 1 $\pi_{xg}$



Table V. Qualitative Character of the CASSCF Orbitals for  
 $\text{NO} + \text{N} \rightarrow \text{N}_2 + \text{O}$ ,  $^3\text{A}'$  Surface

orbital	reactants	saddle point	products
7a'	NO5 $\sigma$	NO5 $\sigma$	N <sub>2</sub> 1 $\pi_{yu}$
8a'	NO1 $\pi_y$	NO1 $\pi_y$	N <sub>2</sub> 3 $\sigma_g$
9a'	N2p <sub>z</sub>	N2p <sub>z</sub>	O2p <sub>z</sub>
10a'	N2p <sub>y</sub>	N2p <sub>y</sub>	O2p <sub>y</sub>
11a'	NO2 $\pi_y$	NO2 $\pi_y$	N <sub>2</sub> 3 $\sigma_u$
12a'	NO6 $\sigma$	NO6 $\sigma$	N <sub>2</sub> 1 $\pi_{yg}$
1a''	NO1 $\pi_x$	NO1 $\pi_x$	O2p <sub>x</sub>
2a''	N2p <sub>x</sub>	NO2 $\pi_x$ + N2p <sub>x</sub>	N <sub>2</sub> 1 $\pi_{xu}$
3a''	NO2 $\pi_x$	NO2 $\pi_x$ - N2p <sub>x</sub>	N <sub>2</sub> 1 $\pi_{xg}$

•

Table VI. Computed Spectroscopic Constants for O<sub>2</sub>, NO, and N<sub>2</sub><sup>a</sup>.

	O <sub>2</sub>				NO				N <sub>2</sub>			
	$r_e$	$\omega_e$	$D_0$		$r_e$	$\omega_e$	$D_0$		$r_e$	$\omega_e$	$D_0$	
[5s3p2d]				CCI + Q	2.291	1580	4.537		2.076	2381	9.187	
supermolecule				CASSCF	2.307	1522	3.634		2.083	2359	8.618	
[5s3p2d]				CCI + Q			4.702					
				SDCI + Q			4.783					
				CCI + Q + 2s			4.598					
[5s3p2d1f]				CCI + Q			4.973		2.078	2383	9.595	
				SDCI + Q				6.443			9.602	
				CCI + Q + 2s							9.190	
Experiment	2.282	1580	5.116		2.175	1904	6.497		2.704	2359	9.759	

<sup>a</sup>  $r_e$  in a<sub>0</sub>,  $\omega_e$  in cm<sup>-1</sup>, and  $D_0$  in eV.

Table VII. Computed Potential Surface Properties for  $N + O_2 \rightarrow NO + O^a$ .

		$^2A'$		$^4A'$	
		CCI + Q	CASSCF	CCI + Q	CASSCF
$\Delta E_{rx}^b$	[5s3p2d]	-30.9	-35.0	-30.9	-35.0
$\Delta E_b^c$	[5s3p2d]	13.4	19.7	20.6	28.4
	[5s3p2d1f]	11.9	18.4	19.1	27.1
	ext. CCI	11.7		19.5	
	best estimate	10.2		18.0	
saddle point	$r_{NO}$	3.441	3.269	3.310	3.154
geometry <sup>d</sup>	$r_{OO}$	2.329	2.368	2.359	2.434
	$\theta_{NOO}$	115.0	114.1	109.4	109.9
saddle point	$\omega_1$	1498.	1294.	1406.	1187.
frequencies	$\omega_2$	370.	367.	367.	365.
	$\omega_3$	505. <i>i</i>	702. <i>i</i>	689. <i>i</i>	612. <i>i</i>
zero point		0.44	0.13	0.30	-.02
correction					
corrected		10.6	18.5	18.3	27.1
$\Delta E_b$					

<sup>a</sup> Energy quantities are in kcal/mole and geometries are in  $a_0$ .

<sup>b</sup> Heat of Reaction. The heat of reaction for  $N + O_2$  was obtained from the supermolecule  $D_e$ 's for  $O_2$  and  $NO$  given in Table VI.

<sup>c</sup> Barrier Height.

<sup>d</sup> Using the ext. CCI the saddle point location for  $\theta = 110^\circ$  is  $r_{NO} = 3.433$  and  $r_{OO} = 2.354$ . The barrier height at this saddle point location is 11.76 kcal/mole.

Table VIII. Minimum Energy Path for  $N + O_2 \rightarrow NO + O, {}^2A'$  surface.<sup>a,b</sup>

CASSCF			CCI + Q			Ext. CCI + Q		
$r_{NO}$	$r_{OO}$	Energy	$r_{NO}$	$r_{OO}$	Energy	$r_{NO}$	$r_{OO}$	Energy
20.0	2.313	-204.15389	20.0	2.295	-204.35700	20.0	2.291	-204.36861
3.70	2.332	-204.13030	3.70	2.299	-204.33777	3.70	2.299	-204.35202
3.50	2.344	-204.12516	3.50	2.326	-204.33588	3.50	2.326	-204.34991
3.30	2.365	-204.12247	3.30	2.344	-204.33660	3.30	2.344	-204.35025
3.10	2.408	-204.12370	3.10	2.371	-204.34160	3.10	2.371	-204.35479
2.90	2.452	-204.13084	2.90	2.412	-204.34959	2.90	2.412	-204.36351
2.687	2.444	-204.14017				2.687	2.444	-204.37579
2.449	2.507	-204.14740				2.449	2.507	-204.38615
2.378	2.572	-204.14797				2.378	2.572	-204.38873
2.300	2.737	-204.14718				2.300	2.737	-204.39437
2.206	2.998	-204.15806				2.206	2.998	-204.39738
2.205	3.50	-204.18523						
2.218	4.00	-204.19868						

<sup>a</sup>  $\theta_{NOO} = 110^\circ$

<sup>b</sup> All quantities are in atomic units.

Table IX. Minimum Energy Path for  $\text{N} + \text{O}_2 \rightarrow \text{NO} + \text{O}$ ,  $^4\text{A}'$  Surface<sup>a,b</sup>

CASSCF			CCI + Q		
$r_{\text{NO}}$	$r_{\text{OO}}$	Energy	$r_{\text{NO}}$	$r_{\text{OO}}$	Energy
20.0	2.313	-204.15389	20.0	2.295	-204.35700
3.50	2.350	-204.11602	3.50	2.331	-204.32602
3.30	2.382	-204.10961	3.30	2.361	-204.32602
3.10	2.454	-204.10863	3.10	2.415	-204.32544
2.90	2.516	-204.11190	2.90	2.466	-204.32991

<sup>a</sup>  $\theta_{\text{NOO}} = 110^\circ$

<sup>b</sup> All quantities are in atomic units.

Table X. Computed Potential Surface Properties for  $N + NO \rightarrow N_2 + O$

		$^3A''$		$^3A'$	
		CCI + Q	CASSCF	CCI + Q	CASSCF
$\Delta E_{rx}^b$	[5s3p2d]	-77.0	-80.6	-77.0	-80.6
$\Delta E_b^c$	[5s3p2d]	1.3	7.6	16.6	28.1
	[5s3p2d1f]	0.5	5.0	14.4	25.3
saddle point	$r_{NN}$	4.102	3.438	3.574	3.324
geometry	$r_{NO}$	2.172	2.197	2.210	2.250
	$\theta_{NNO}$	108.9	108.5	116.5	116.5
saddle point	$\omega_1$	1785.	1720.	1678.	1586.
frequencies	$\omega_2$	385.	396.	383.	383.
	$\omega_3$	210. <i>i</i>	250. <i>i</i>	569. <i>i</i>	727. <i>i</i>
zero point		0.47	0.39	0.31	0.18
correction					
corrected		1.0	5.4	14.7	25.5
$\Delta E_b$					

<sup>a</sup> Energy quantities are in kcal/mole and geometries are in  $a_0$ .

<sup>b</sup> Heat of Reaction.

<sup>c</sup> Barrier Height.

Table XI. Minimum Energy Path for  $\text{N} + \text{NO} \rightarrow \text{N}_2 + \text{O}$ ,  $^3\text{A}''$  surface<sup>a,b</sup>

CASSCF			CCI + Q		
$r_{\text{NN}}$	$r_{\text{NO}}$	Energy	$r_{\text{NN}}$	$r_{\text{NO}}$	Energy
20.0	2.192	-183.80080	20.0	2.182	-183.95325
4.50	2.189	-183.79601	4.50	2.177	-183.95185
4.00	2.187	-183.79171	4.00	2.174	-183.95113
3.50	2.197	-183.78875	3.50	2.188	-183.95384
3.00	2.243	-183.79137	3.00	2.242	-183.96240

<sup>a</sup>  $\theta_{\text{NNO}} = 110^\circ$

<sup>b</sup> All quantities are in atomic units.

Table XII. Minimum Energy Path for  $\text{N} + \text{NO} \rightarrow \text{N}_2 + \text{O}$ ,  $^3\text{A}'$  surface<sup>a,b</sup>

CASSCF			CCI + Q		
$r_{\text{NN}}$	$r_{\text{NO}}$	Energy	$r_{\text{NN}}$	$r_{\text{NO}}$	Energy
20.0	2.20	-183.80109	20.0	2.20	-183.95330
4.50	2.192	-183.79096	4.50	2.184	-183.94585
4.00	2.195	-183.77798	4.00	2.187	-183.93577
3.50	2.210	-183.75720	3.50	2.196	-183.92708
3.00	2.264	-183.75941	3.00	2.239	-183.94257

<sup>a</sup>  $\theta_{\text{NNO}} = 110^\circ$

<sup>b</sup> All quantities are in atomic units.



Figure Captions.

Fig. 1. A plot of the global CASSCF potential surface for the  $^2A'$  state of the  $N + O_2 \rightarrow NO + O$  reaction.

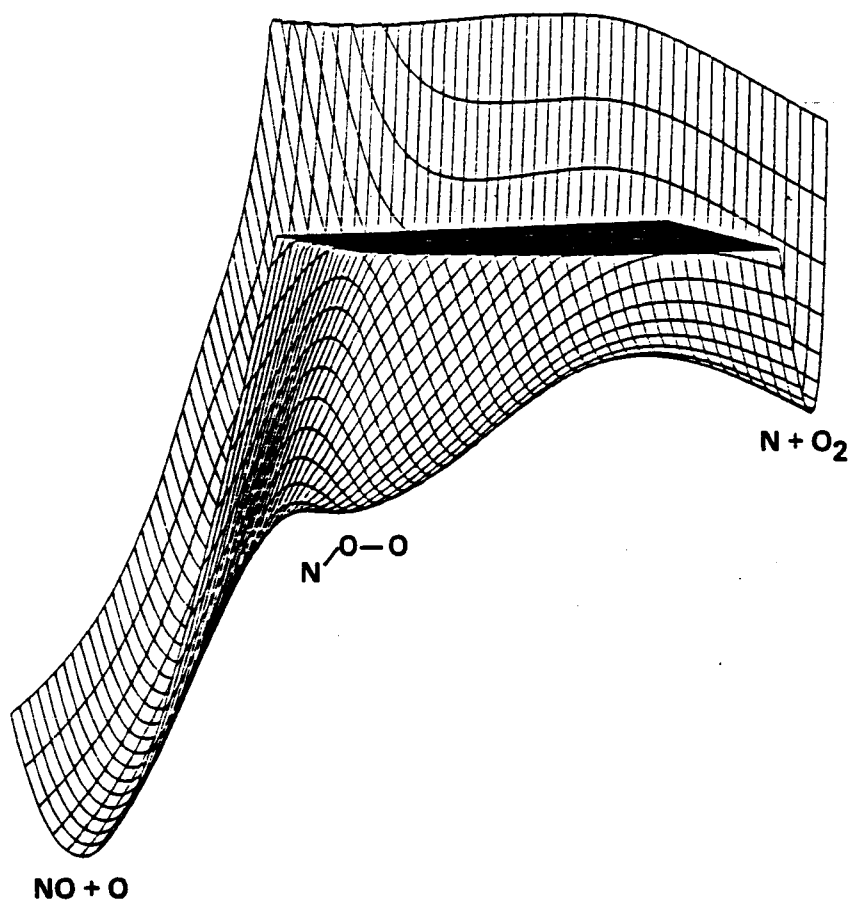
Fig. 2. Bending potentials for the saddle point region of the  $^2A'$  and  $^4A'$  surfaces of the  $N + O_2 \rightarrow NO + O$  reaction. The bending potentials are shown for both CASSCF and CCI + Q.

Fig. 3. Bending potentials for the saddle point region of the  $^3A'$  and  $^3A''$  surfaces of the  $O + N_2 \rightarrow NO + N$  reaction. The bending potentials are shown for both CASSCF and CCI + Q.

Fig. 4. Energy along the minimum energy path for the  $^3A''$  and  $^3A'$  surfaces for  $NO + N$  for both CASSCF and CCI wave functions.

Fig. 1

**$^2A'$  CASSCF POTENTIAL SURFACE  
FOR  $N + O_2 \longrightarrow NO + O$**



WALCH

Fig. 2

### N-O-O BENDING POTENTIALS

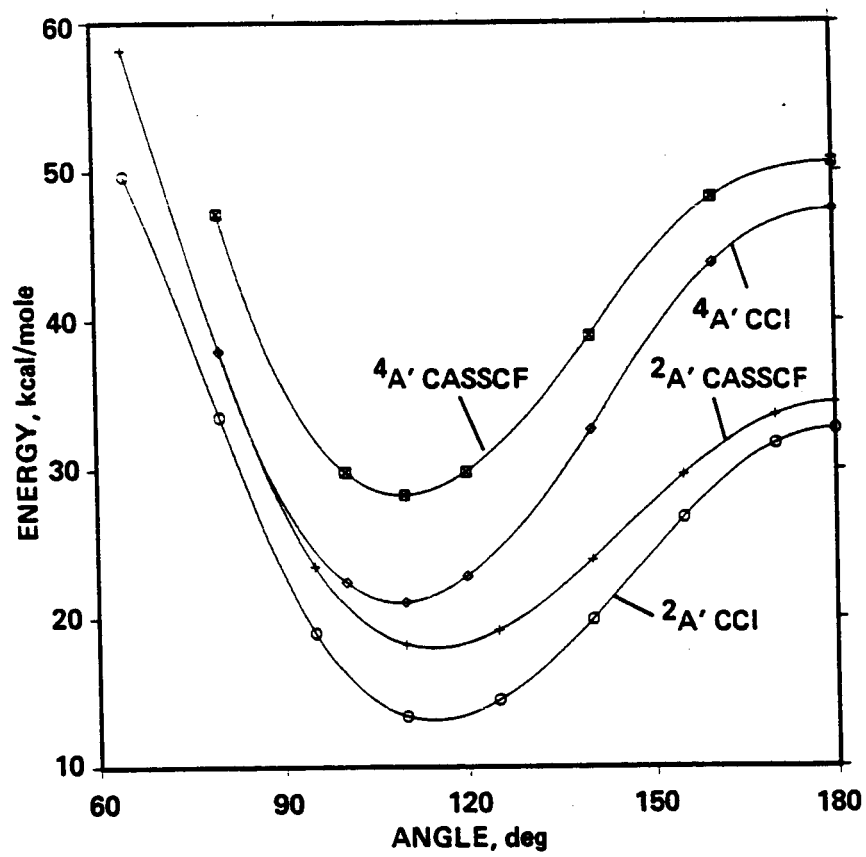


Fig. 3

### O-N-N BENDING POTENTIALS

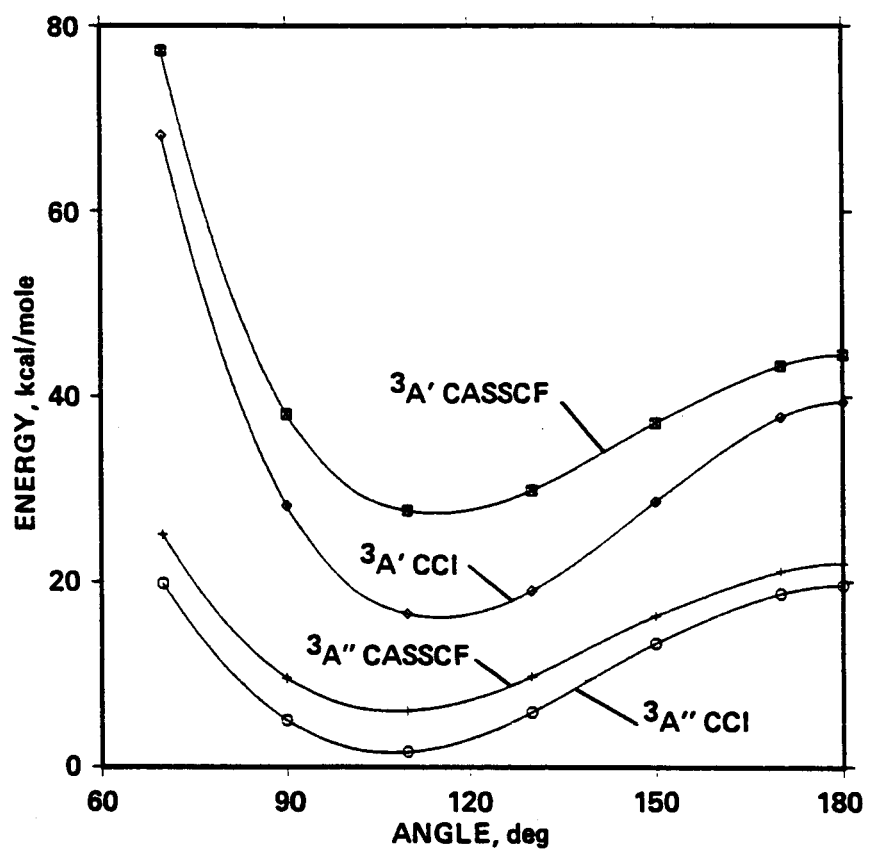
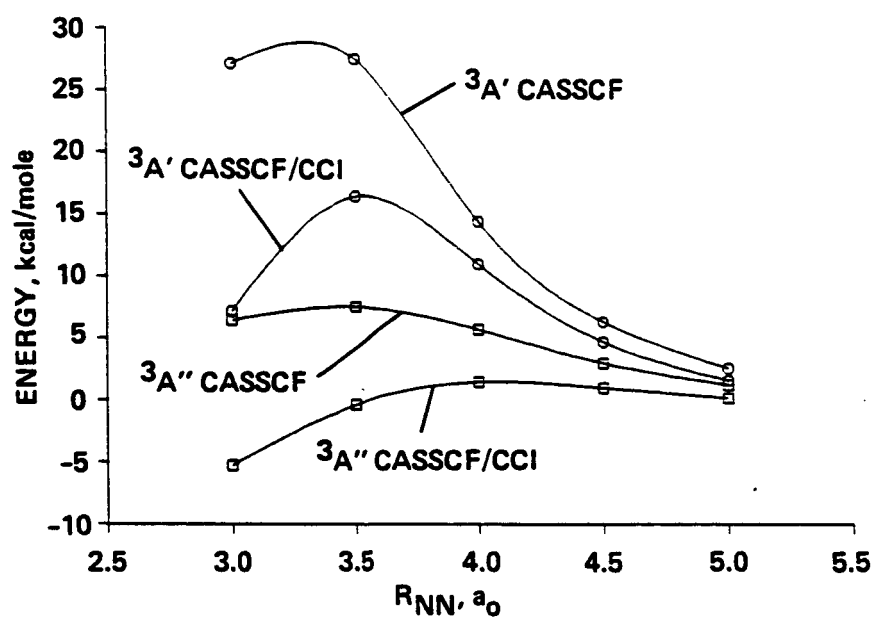


Fig. 4



Appendix. The appendix contains tables of the computed energies. In the following tables, all distances and energies are in atomic units and  $\theta$  is degrees. See the text for a description of the computational method.

Table AI. Energies for The  $N + O_2 \rightarrow NO + O$  Reaction

$^2A'$ Surface				
$\theta$	$r_{NO}$	$r_{OO}$	E(CASSCF)	E(CCI + Q)
110.0	20.000	2.500	-204.14355	-204.34412
110.0	20.000	2.400	-204.15107	-204.35290
110.0	20.000	2.282	-204.15353	-204.35694
110.0	20.000	2.200	-204.14913	-204.35369
110.0	20.000	2.100	-204.13392	-204.34202
110.0	20.000	20.000	-204.01675	-204.18666
110.0	3.700	2.750	-204.09542	-204.29479
110.0	3.700	2.600	-204.11227	-204.31487
110.0	3.700	2.450	-204.12534	-204.32704
110.0	3.700	2.300	-204.12994	-204.33777
110.0	3.700	2.150	-204.11859	-204.32742
110.0	3.700	2.000	-204.07903	-204.29269
110.0	3.500	2.750	-204.09465	-204.29739
110.0	3.500	2.600	-204.10975	-204.31577
110.0	3.500	2.450	-204.12123	-204.33003
110.0	3.500	2.300	-204.12450	-204.33562
110.0	3.500	2.150	-204.11213	-204.32410
110.0	3.500	2.000	-204.07199	-204.28825
110.0	3.300	2.750	-204.09802	-204.30469
110.0	3.300	2.600	-204.11087	-204.32072
110.0	3.300	2.450	-204.12001	-204.33259
110.0	3.300	2.300	-204.12104	-204.33589
110.0	3.300	2.150	-204.10676	-204.32300
110.0	3.300	2.000	-204.06522	-204.28427
110.0	3.100	2.750	-204.10603	-204.31609
110.0	3.100	2.600	-204.11679	-204.33012
110.0	3.100	2.450	-204.12336	-204.33942

110.0	3.100	2.300	-204.12154	-204.33981
110.0	3.100	2.150	-204.10439	-204.32437
110.0	3.100	2.000	-204.06031	-204.28102
110.0	2.900	3.000	-204.09801	
110.0	2.900	2.750	-204.11730	
110.0	2.900	2.600	-204.12646	-204.34208
110.0	2.900	2.450	-204.13084	-204.34929
110.0	2.900	2.300	-204.12622	-204.34689
110.0	2.900	2.150	-204.10579	-204.32818
110.0	2.700	4.000	-204.12817	
110.0	2.700	3.500	-204.11330	
110.0	2.700	3.000	-204.11256	
110.0	2.700	2.750	-204.12945	
110.0	2.700	2.600	-204.13720	
110.0	2.700	2.450	-204.13971	
110.0	2.700	2.400	-204.13869	
110.0	2.700	2.300	-204.13262	
110.0	2.700	2.000	-204.05765	
110.0	2.500	4.000	-204.16464	
110.0	2.500	3.500	-204.14941	
110.0	2.500	3.000	-204.13112	
110.0	2.500	2.800	-204.13819	
110.0	2.500	2.750	-204.14046	
110.0	2.500	2.600	-204.14570	
110.0	2.500	2.450	-204.14581	
110.0	2.500	2.400	-204.14394	
110.0	2.500	2.282	-204.13389	
110.0	2.500	2.000	-204.05365	
110.0	2.200	4.000	-204.19854	
110.0	2.200	3.500	-204.18522	
110.0	2.200	3.000	-204.15834	
110.0	2.200	2.750	-204.14585	



110.0	2.200	2.600	-204.14198	
110.0	2.200	2.450	-204.13436	
110.0	2.200	2.300	-204.11750	
110.0	2.200	2.000	-204.02003	
110.0	2.000	4.000	-204.17823	
110.0	2.000	3.500	-204.16801	
110.0	2.000	3.000	-204.14086	
110.0	2.000	2.750	-204.11848	
110.0	2.000	2.600	-204.10581	
110.0	2.000	2.300	-204.06444	
110.0	2.000	2.000	-203.95082	
130.0	3.300	2.300	-204.11527	
120.0	3.300	2.300	-204.12047	
100.0	3.300	2.300	-204.11561	
90.0	3.300	2.300	-204.10234	
115.0	3.441	2.329	-204.12389	-204.33567
180.0	3.500	2.300	-204.09866	-204.30487
170.0	3.500	2.300	-204.09997	-204.30642
155.0	3.500	2.300	-204.10631	-204.31432
140.0	3.500	2.300	-204.11543	-204.32524
80.0	3.500	2.300	-204.09295	-204.30351
65.0	3.500	2.300	-204.06082	-204.27772
125.0	3.500	2.300	-204.12296	-204.33385
125.0	3.300	2.300	-204.11837	-204.33307
125.0	3.700	2.300	-204.12926	-204.33694
125.0	3.500	2.100	-204.10220	-204.31457
125.0	3.500	2.500	-204.11530	-204.32282
125.0	3.300	2.500	-204.11307	-204.32467
125.0	3.300	2.100	-204.09593	-204.31290
125.0	3.100	2.300	-204.11795	-204.33625
125.0	3.700	2.100	-204.10926	-204.31982
125.0	3.700	2.500	-204.12028	-204.32433

95.0	3.500	2.300	-204.11609	-204.32667
95.0	3.300	2.300	-204.11011	-204.32490
95.0	3.700	2.300	-204.12364	-204.33076
95.0	3.500	2.100	-204.09268	-204.30678
95.0	3.500	2.500	-204.11151	-204.31945
95.0	3.300	2.500	-204.10984	-204.32172
95.0	3.100	2.300	-204.10783	-204.32659
95.0	3.300	2.100	-204.08299	-204.30044
95.0	3.700	2.100	-204.10221	-204.31351
95.0	3.700	2.500	-204.11638	-204.32079

Table AII. Energies for The  $N + O_2 \rightarrow NO + O$  Reaction

---



---

<sup>4</sup> A' Surface				
$\theta$	$r_{NO}$	$r_{OO}$	E(CASSCF)	E(CCI + Q)
110.0	2.900	2.600	-204.11047	-204.32589
110.0	2.900	2.450	-204.11104	-204.32985
110.0	2.900	2.300	-204.10257	-204.32372
110.0	2.900	2.150	-204.07811	-204.30111
110.0	3.100	2.600	-204.10472	-204.31883
110.0	3.100	2.450	-204.10863	-204.32520
110.0	3.100	2.300	-204.10433	-204.32291
110.0	3.100	2.150	-204.08485	-204.30486
110.0	3.300	2.600	-204.10136	-204.31208
110.0	3.300	2.450	-204.10881	-204.32185
110.0	3.300	2.300	-204.10845	-204.32337
110.0	3.300	2.150	-204.09297	-204.30841
110.0	3.500	2.600	-204.10203	-204.30888
110.0	3.500	2.450	-204.11258	-204.32173
110.0	3.500	2.300	-204.11515	-204.32574
110.0	3.500	2.150	-204.10219	-204.31622
180.0	3.300	2.300	-204.07296	-204.28140
160.0	3.300	2.300	-204.07667	-204.28711
140.0	3.300	2.300	-204.09144	-204.30489
120.0	3.300	2.300	-204.10594	-204.32058
100.0	3.300	2.300	-204.10600	-204.32122
80.0	3.300	2.300	-204.07837	-204.29650
109.4	3.310	2.359	-204.11015	-204.32422

Table AIII. Energies for The  $O + N_2 \rightarrow NO + N$  Reaction

---



---

$^3A''$ Surface				
$\theta$	$r_{NO}$	$r_{NN}$	E(CASSCF)	E(CCI + Q)
110.0	2.400	20.000	-183.78330	-183.93381
110.0	2.300	20.000	-183.79517	-183.94655
110.0	2.200	20.000	-183.80077	-183.95309
110.0	2.100	20.000	-183.79674	-183.95006
110.0	2.000	20.000	-183.77843	-183.93281
90.0	2.175	20.000	-183.80125	
110.0	20.000	20.000	-183.60731	-183.73305
110.0	2.400	4.500	-183.77828	-183.93210
110.0	2.400	4.000	-183.77419	-183.93152
110.0	2.400	3.500	-183.77362	-183.93746
110.0	2.400	3.000	-183.78342	-183.95445
110.0	2.300	4.500	-183.79017	-183.94485
110.0	2.300	4.000	-183.78587	-183.94406
110.0	2.300	3.500	-183.78404	-183.94840
110.0	2.300	3.000	-183.78992	-183.96090
110.0	2.200	5.000	-183.79874	-183.95288
110.0	2.200	4.500	-183.79595	-183.95160
110.0	2.200	4.000	-183.79163	-183.95083
110.0	2.200	3.500	-183.78875	-183.95378
110.0	2.200	3.000	-183.79052	-183.96160
110.0	2.100	4.500	-183.79231	-183.94911
110.0	2.100	4.000	-183.78823	-183.94867
110.0	2.100	3.500	-183.78458	-183.95046
110.0	2.100	3.000	-183.78205	-183.95335
110.0	2.000	4.500	-183.77473	-183.93531
110.0	2.000	4.000	-183.77121	-183.93617
110.0	2.000	3.500	-183.76717	-183.93693

110.0	2.000	3.000	-183.76011	-183.93172
90.0	2.175	4.000	-183.78604	
120.0	2.175	4.000	-183.78992	
150.0	2.175	4.000	-183.77538	
100.0	2.200	4.500	-183.79559	-183.95130
100.0	2.200	4.000	-183.79062	-183.94997
100.0	2.200	3.500	-183.78663	-183.95203
120.0	2.200	4.500	-183.79498	-183.95047
120.0	2.200	4.000	-183.78974	-183.94859
120.0	2.200	3.500	-183.78510	-183.94977
180.0	2.200	4.000	-183.76623	-183.92216
170.0	2.200	4.000	-183.76764	-183.92359
150.0	2.200	4.000	-183.77528	-183.93215
130.0	2.200	4.000	-183.78574	-183.94402
90.0	2.200	4.000	-183.78600	-183.94541
70.0	2.200	4.000	-183.76124	-183.92177
108.9	2.172	4.102	-183.79272	-183.95133
110.0	2.150	4.000	-183.79132	
110.0	2.150	3.750	-183.78931	
110.0	2.200	3.750	-183.78970	
110.0	2.300	3.750	-183.78422	
110.0	2.150	3.500	-183.78802	
110.0	2.200	3.500	-183.78875	
110.0	2.300	3.500	-183.78404	
110.0	2.150	3.250	-183.78764	
110.0	2.200	3.250	-183.78916	
110.0	2.300	3.250	-183.78602	
110.0	2.150	3.000	-183.78766	
110.0	2.200	3.000	-183.70052	
110.0	2.300	3.000	-183.78992	
130.0	3.000	2.200	-183.83306	
110.0	3.500	2.200	-183.87763	

130.0	3.500	2.200	-183.87906	
150.0	3.500	2.200	-183.87666	
130.0	4.000	2.200	-183.90618	
90.0	20.000	2.300	-183.90302	-184.04786
90.0	20.000	2.200	-183.92068	-184.06625
90.0	20.000	2.100	-183.92915	-184.07564
90.0	20.000	2.000	-183.92372	-184.07127
90.0	20.000	1.900	-183.89795	-184.04668

Table AIV. Energies for The  $O + N_2 \rightarrow NO + N$  Reaction

$^3A'$ Surface				
$\theta$	$r_{NO}$	$r_{NN}$	E(CASSCF)	E(CCI + Q)
110.0	2.200	20.000	-183.80109	-183.95330
110.0	2.400	4.500	-183.77369	-183.92704
110.0	2.400	4.000	-183.76149	-183.91802
110.0	2.400	3.500	-183.74421	-183.91249
110.0	2.400	3.000	-183.75507	-183.93458
110.0	2.300	4.500	-183.78542	-183.93945
110.0	2.300	4.000	-183.77280	-183.92984
110.0	2.300	3.500	-183.75354	-183.92247
110.0	2.300	3.000	-183.75889	-183.94088
110.0	2.200	5.000	-183.79692	-183.95067
110.0	2.200	4.500	-183.79093	-183.94573
110.0	2.200	4.000	-183.77797	-183.93569
110.0	2.200	3.500	-183.75715	-183.92707
110.0	2.200	3.000	-183.75776	-183.94186
110.0	2.100	4.500	-183.78686	-183.94253
110.0	2.100	4.000	-183.77366	-183.93223
110.0	2.100	3.500	-183.75174	-183.92322
110.0	2.100	3.000	-183.74858	-183.93369
110.0	2.000	4.500	-183.76860	-183.92524
110.0	2.000	4.000	-183.75530	-183.91493
110.0	2.000	3.500	-183.73289	-183.90679
110.0	2.000	3.000	-183.72711	-183.91248
180.0	2.200	3.500	-183.73027	-183.89056
170.0	2.200	3.500	-183.73211	-183.89314
150.0	2.200	3.500	-183.74202	-183.90772
130.0	2.200	3.500	-183.75360	-183.92309
90.0	2.200	3.500	-183.74054	-183.90841

70.0	2.200	3.500	-183.67801	-183.84481
116.5	2.210	3.574	-183.76030	-183.92696
130.0	3.000	2.200	-183.82618	
130.0	3.500	2.200	-183.87385	
150.0	4.000	2.200	-183.90082	
130.0	4.000	2.200	-183.90161	
110.0	4.000	2.200	-183.90108	
90.0	4.000	2.200	-183.89571	
130.0	5.000	2.200	-183.91812	
90.0	20.000	2.200	-183.92066	